Urban Emissions of Water Vapor in Winter

Olivia E. Salmon[1], Paul B. Shepson[1,2], Xinrong Ren[3,4], Allison B. Marquardt Collow[5,6], Mark A. Miller[7], Annmarie G. Carlton[8], Maria O. L. Cambaliza[1,9], Alexie Heimburger[1], Kristan L. Morgan[2], Jose D. Fuentes[10], Brian H. Stirm[11], Robert Grundman II[11], Russell R. Dickerson[4]

[1]Department of Chemistry, Purdue University, West Lafayette, Indiana, USA, [2]Department of Earth, Atmospheric, and Planetary Sciences and Purdue Climate Change Research Center, Purdue University, West Lafayette, Indiana, USA, [3]Air Resources Laboratory, National Oceanic and Atmospheric Administration, College Park, Maryland, USA, [4]Department of Atmospheric and Oceanic Science, University of Maryland, College Park, Maryland, USA, [5]Universities Space Research Association, Columbia, Maryland, USA, [6]NASA/GSFC Code 610.1, Global Modeling and Assimilation Office, Greenbelt, Maryland, USA, [7]Department of Environmental Sciences, Rutgers University, New Brunswick, New Jersey, USA, [8]Department of Chemistry, University of California, Irvine, California, USA, [9]Now at the Department of Physics, Ateneo de Manila University, Quezon City, Philippines, [10]Department of Meteorology, The Pennsylvania State University, University Park, Pennsylvania, USA, [11]School of Aviation and Transportation Technology, Purdue University, West Lafayette, Indiana, USA

Corresponding author: Olivia E. Salmon (osalmon@purdue.edu)

Key Points:

- Unique airborne data reveals elevated H_2O_v mole fractions downwind of urban areas in winter months
- Estimates of H_2O_v emitted from fossil fuel combustion account for less than 10% of the observed H_2O_v enhancement in the urban outflow
- Combustion and evaporative cooling cannot account for the urban H_2O_v excess, leaving enhanced urban evaporation as a plausible explanation

Abstract

Elevated water vapor (H_2O_v) mole fractions were occassionally observed downwind of Indianapolis, IN, and the Washington, D.C.-Baltimore, MD, area during airborne mass balance experiments conducted during winter months between 2012 and 2015. On days when an urban H_2O_v excess signal was observed, H_2O_v emissions estimates range between 1.6×10^4 and 1.7×10^5 kg s^{-1}, and account for up to 8.4% of the total (background + urban excess) advected flow of atmospheric boundary layer H_2O_v from the urban study sites. Estimates of H_2O_v emissions from combustion sources and electricity generation facility cooling towers are 1-2 orders of magnitude smaller than the urban H_2O_v emission rates estimated from observations. Instances of urban H_2O_v enhancement could be a result of differences in snowmelt and evaporation rates within the urban area, due in part to larger wintertime anthropogenic heat flux and land cover differences, relative to surrounding rural areas. More study is needed to understand why the urban H_2O_v excess signal is observed on some days, and not others. Radiative transfer modeling indicates that the observed urban enhancements in H_2O_v and other greenhouse gas mole fractions contribute only $0.1^oC\ day^{-1}$ to the urban heat island at the surface. This integrated warming through the boundary layer is offset by longwave cooling by H_2O_v at the top of the boundary layer. While the radiative impacts of urban H_2O_v emissions do not meaningfully influence urban heat island intensity, urban H_2O_v emissions may have the potential to alter downwind aerosol and cloud properties.

1. Introduction

Gradients in humidity between urban and rural environments have been observed for decades, with cities found to be both drier and more humid than surrounding rural areas depending on time of day or year [*Kuttler et al.*, 2007; *Liu et al.,* 2009; *Hall et al*., 2016]. In general, cities are expected to be drier during the day than surrounding rural areas [*Arnfield,* 2003]. Soil and vegetation retain moisture and are capable of larger rates of evapotranspiration, in contrast to impervious urban surfaces like asphalt and concrete. Instances when urban atmospheric moisture levels are in excess of rural areas, referred to as urban moisture excess (UME), are often observed at night when urban heat islands (UHIs) are at their strongest, if dew point temperatures are reached in the surrounding rural area but not the city [*Hage*, 1975; *Bornstein and Tam,* 1977; *Holmer and Eliasson*, 1999; *Deosthali*, 2000; *Kuttler et al.,* 2007]. Additionally, UME events have been observed during the daytime in mid-latitude cities during winter months [*Hage,* 1975; *Ackerman,* 1987], and in some cities throughout the year [*Kuttler et al.,* 2007; *Hall et al.,* 2016].

These gradients are frequently rooted in differences between urban and rural energy balance and moisture sources [*Arnfield*, 2003]. Faster rates of snowmelt and local advection-assisted evapotranspiration have been reported in urban areas [*Oke,* 1979; *Oke and McCaughey*, 1983; *Oke et al.,* 1992; *Bengtsson and Westerström*, 1992; *Neumann and Marsh,* 1998; *Moriwaki and Kanda,* 2004]. Energy flux partitioning in urban areas is sensitive to the Bowen ratio (ratio of sensible to latent heat flux), which is low following precipitation events [*Offerle et al.,* 2006; *Ward et al.,* 2013; *Ramamurthy et al.,* 2014; *Ao et al.,* 2016]. Urban latent heat fluxes during the winter-spring transition can respond strongly to soil moisture thaw and snowmelt [*Offerle et al.,* 2006; *Lemonsu et al.,* 2008; *Leroyer et al.,* 2010]. However, suburban and urban areas within the same city can exhibit different relationships between latent heat flux and the physical state and availability of moisture on and within impervious and vegetated land cover [*Bergeron and Strachan,* 2012]. Direct anthropogenic emissions of heat and moisture from combustion sources, industry, and home heating and cooling have been reported to be significant [*Hage,* 1972; *Grimmond,* 1992; *Moriwaki et al.,* 2008; *Sailor,* 2011; *Gorski et al.,* 2015], and have also been implicated as contributors to UME [*Hage,* 1972, 1975; *Bornstein and Tam,* 1977; *Ackerman,* 1987]. Bergeron and Strachan [2012] estimate that wintertime water vapor (H_2O_v) emissions in Montreal exceed that of rural areas by over 50% due to combustion and sublimation/evaporation

of snow from roofs and roads, and Gorski et al. [2015] estimate that combustion H_2O_v can account for up to 13% of surface-level H_2O_v in Salt Lake City in winter.

In addition to instances of UME, annual maxima in greenhouse gas (GHG) mole fractions, such as for carbon dioxide (CO_2) and methane (CH_4), are observed in mid-latitude cities in winter when energy consumption is high, vertical mixing is poor, and boundary layer heights are low [*Christen*, 2014; *Energy Information Administration (EIA*), 2015; *McKain et al.,* 2015; *Moore and Jacobson,* 2015]. Few studies have considered the impact of elevated mole fractions of H_2O_v and other GHGs on urban temperatures by absorption and re-emission of longwave radiation [*Oke et al.,* 1991; *Holmer and Eliasson,* 1999; *McCarthy et al.,* 2010]. UHI formation has been temporally linked with UME [*Holmer and Eliasson,* 1999; *Deosthali,* 2000; *Kuttler et al.,* 2007]. Studies that have quantified the radiative impacts of GHGs on UHI intensity have considered the effect of increasing longwave radiation by 40 Wm^{-2} (informed by urban observervations of the longwave contribution from GHGs) for idealized cities [*Oke et al.,* 1991], as well as the impact of observed urban vapor pressure enhancements (3 hPa) on the Göteborg, Sweeden UHI [*Holmer and Eliasson,* 1999], and the impact of increasing average global CO_2 concentrations to 645 ppm on global megacity UHIs [*McCarthy et al.,* 2010].

Understanding how urban emissions of H_2O_v and other GHGs influence the environment is important, as cities, despite covering only 3% of the Earth's land surface, are responsible for 70% of global CO_2 emissions and house 54% of the world's population, with these numbers projected to grow in the coming decades [*Center for International Earth Science Information Network,* 2011; *United Nations,* 2011; *World Health Organization,* 2016]. A positive atmospheric H_2O_v feedback exists in response to increased CO_2 concentrations, with models suggesting H_2O_v is responsible for a significant portion of warming via radiative effects [*Rind et al.,* 1991; *Willet et al.,* 2007]. Furthermore, it has been shown that atmospheric concentrations of H_2O_v are increasing and influence the rate of warming [*Solomon et al.,* 2010; *Chung et al.,* 2014]. However, questions still remain about local scale influences of H_2O_v emissions, and their magnitude.

Urban H_2O_v excess emissions could influence aerosol properties and the associated population of cloud condensation nuclei (CCN) which could also modify cloud cover and weather downwind of urban areas [*Mölders and Olson,* 2004; *Kreidenweis et al.,* 2005; *Bréon,* 2006; *Rosenfeld et al.,* 2008; *Trusilova et al.,* 2008; *Twohy et al.,* 2009; *Kourtidis et al.,* 2015]. In

addition to regional effects on cloud cover and water cycling, enhanced H_2O_v mole fraction impacts the liquid water content of aerosols. As discussed in recent publications, aerosol liquid water content has a significant impact on the processing of pollutants that partition to the aerosol phase, or the evolution of secondary organic aerosol (SOA) and climate-relevant aerosol properties [*Carlton and Turpin,* 2013; *Hodas et al.,* 2014; *Guo et al.,* 2015; *Nguyen et al.,* 2015; *Rindelaub et al.,* 2015].

Here we discuss our airborne case studies of elevated H_2O_v mole fractions observed downwind of (1) the Washington, D.C.- Baltimore, MD, metropolitan area (D.C.-Balt), collected as part of the Wintertime Investigation of Emissions, Reactivity, and Transport (WINTER) and Fluxes of Atmospheric Greenhouse Gases in Maryland (FLAGG-MD) campaigns, and (2) Indianapolis, IN, as part of the ongoing Indianapolis Flux Experiment (INFLUX). Unlike past studies that have reported urban H_2O_v excess by comparing measurements from tower sites or surface-mobile traverses [*Hage*, 1975; *Holmer and Eliasson*, 1999; *Deosthali*, 2000; *Richards*, 2005; *Kuttler et al.,* 2007; *Liu et al.,* 2009; *Hall et al*., 2016], this study represents the first reported observations and quantification of city-wide enhancements in H_2O_v mole fractions during daytime. Additionally, we report emission rates of urban-derived H_2O_v from our mass balance experiments conducted in the two cities, and discuss possible sources. We test the hypothesis that elevated H_2O_v, CO_2, and CH_4 mole fractions within an urban center influence the UHI via direct radiative effects, and discuss potential impacts of urban H_2O_v emissions on areas within and downwind of cities.

2. Methods

2.1. Site Description

Airborne experiments were conducted above D.C.-Balt, the urban area centered around the cities of Washington, D.C. (38.905°N, 77.016°W) and Baltimore, MD (39.288°N, 76.617°W), on 13, 19, 20, 23, 25, 27 February and 9, 12 March, 2015 as part of the WINTER and FLAGG-MD campaigns. D.C.-Balt is a U.S. Census Bureau-defined Combined Statistical Area, and has a population of approximately 9.63 million [*U.S. Census Bureau,* 2016]. The population density across D.C.-Balt is spatially variable. The most densely populated areas, at 3806 persons km^{-2} and 2174 persons km^{-2}, are within the city boundaries of Washington, D.C. and Baltimore, MD, respectively, [*US Census Bureau,* 2010]. The urban study site is surrounded by rural land use to the north and south. The Appalachian Mountains lie to the west, and the Chesapeake Bay and Atlantic Ocean lie to the east of the urban area. Northwest winds were commonly observed during the D.C.-Balt flights, which is in line with long-term observations of wintertime winds in the area [*Berg and Allwine,* 2006]. The Washington National Airport reported average temperatures and winds speeds of -0.4°C and 4 m s^{-1}, respectively, during the study period. Airborne observations of urban carbon monoxide, sulfur dioxide, nitrogen dioxide (NO_2), ozone, and aerosol emissions from the D.C.-Balt area have been previously discussed [*He et al.,* 2014; 2016; *Brent et al.,* 2015].

Airborne experiments conducted by Purdue University in Indianapolis, IN (39.791°N, 86.148°W) have been ongoing since 2008 as part of the INFLUX campaign. Indianapolis and its surrounding urban/suburban sprawl have a population of approximately 1.99 million [*US Census Bureau,* 2016], and the population density is 914 persons km^{-2} [*US Census Bureau*, 2010]. The Indianapolis flight experiments discussed herein were conducted in November of 2012 and 2014. The average monthly temperature in Indianapolis in November over these years was 4°C, and winds were from the southwest at 4 m s^{-1} on average, as archived by the National Weather Service. Given its isolation from other urban areas, and its relatively simple meteorology and topography, Indianapolis is an ideal test bed for the development and evaluation of methods to quantify urban emissions from densely populated urban environments. Emissions of CO_2 and CH_4 from Indianapolis are discussed in Mays et al. [2009], Cambaliza et al. [2014, 2015], Lauvaux et al. [2016], and Heimburger et al. [2017].

159

160 2.2. Aircraft Instrumentation

161 The two airborne platforms used to quantify GHG emissions from the urban areas were:
162 Purdue University's Airborne Laboratory for Atmospheric Research (ALAR;
163 http://science.purdue.edu/shepson/research/bai/alar.html) and the UMD's Cessna 402B research
164 aircraft (http://aosc.umd.edu/~flaggmd/). Emission rates of urban H_2O_v excess for D.C.-Balt are
165 estimated from data collected by both aircraft. Emission rates for Indianapolis are estimated from
166 data collected by the ALAR. Table S1 is a flight log that details the date, city, aircraft, low and
167 high temperature, and prior precipitation for all the flights discussed in this text. Purdue's ALAR
168 and the UMD Cessna flew a coordinated flight (here on referred to as the inter-comparison
169 flight) on 19 February 2015. The inter-comparison flight was designed for periods of the
170 experiment to be flown in unison for measurement comparison. Figure S1 shows the ALAR and
171 the UMD Cessna measurements of winds, temperature, pressure, and H_2O_v mole fraction
172 (expressed as mmol mol^{-1}) for a period of the inter-comparison flight in which the aircraft were
173 flying parallel to one another, spaced ~1 km apart, and flying at the same altitude with their
174 heading oriented perpendicular to the mean wind direction.

175

176 2.2.1. Purdue University's Airborne Laboratory for Atmospheric Research

177 Purdue's ALAR is a modified light twin-engine Beechcraft Duchess aircraft equipped
178 with a Best Air Turbulence (BAT) probe for high frequency (50 Hz) three-dimensional wind
179 measurements [*Crawford and Dobosy,* 1992; *Garman et al.,* 2006] installed at the nose of the
180 aircraft. Temperature was measured using a Fast Ultra-Sensitive Temperature (FUST) probe
181 installed on the underside of the BAT probe [*Garman et al.,* 2006]. Flight tracks were recorded
182 using a global positioning system (GPS) and inertial navigation system (INS). During the course
183 of the D.C.-Balt flights, the ALAR was equipped with several gas and aerosol analyzers
184 including: (1) a Picarro G2301-m cavity ring-down spectrometer (CRDS) for 0.5 Hz CO_2, CH_4,
185 and H_2O_v measurements, (2) a Los Gatos Research (LGR) off-axis integrated cavity output
186 spectrometer (OA-ICOS) for 1 Hz NO_2 measurements, and (3) an aerosol spectrometer (model
187 1.109, GRIMM Technologies, Inc., Douglasville, GA) for measurements (6 second intervals) of

188 particle concentration of diameters from 0.25 to 32 μm. The NO_2 and aerosol analyzers were not
189 installed in ALAR at the time of the Indianapolis flight experiments reported here.
190 Instrumentation was housed in a ~1 m^3 volume in the back of the aircraft. A blower installed at
191 the rear of the aircraft pulled ambient air from the inlet at the nose of the aircraft through 5 cm
192 Teflon tubing at a flow rate of 1840 L min^{-1}.

193 For Indianapolis flights, the ALAR Picarro CRDS was calibrated with an in-flight
194 calibration system using National Oceanographic and Atmospheric Association (NOAA) Earth
195 System Research Laboratory analytical standards. For D.C.-Balt flights, the ALAR Picarro
196 CRDS was calibrated according to a Purdue-UMD cross-calibration with analytical CO_2 and CH_4
197 standards from the National Institute of Standards and Technology (NIST). For continuity,
198 Purdue and UMD Picarro CRDS data collected during D.C.-Balt flights were calibrated using
199 NIST standards. After the WINTER campaign, a dew point generator (model LI-610, LiCor Inc.,
200 Lincoln, NE) was used to compare saturation mole fractions to the CRDS H_2O_v measurements.
201 The dew point generator has a reported precision of ±0.01°C for dew point temperature set point.
202 This equates to a maximum variability of $\pm 8 \times 10^{-3}$ mmol mol^{-1} in saturation mole fractions for
203 the dew point temperatures measured. The CRDS-reported H_2O_v mole fractions were ~8% lower
204 than the saturation mole fractions for the set dew point temperatures. Purdue H_2O_v measurements
205 were not calibrated for continuity with the UMD H_2O_v measurements (Figure S1). The Picarro
206 G2301-m instrument has a measured precision of 0.03 ppm and 0.5 ppb for CO_2 and CH_4,
207 respectively (standard deviations (1σ) of 0.5 Hz data over five minutes), for atmospherically
208 relevant trace species mole fractions from dry analytical standards. The measured precision for
209 H_2O_v when sampling humid air from the dew point generator is 3×10^{-2} mmol mol^{-1} for relevant
210 ambient H_2O_v mole fractions. This value is a combination of the precision of the dew point
211 generator output (maximum variability of $\pm 8 \times 10^{-3}$ mmol mol^{-1}) and the CRDS instrument
212 precision.

213

214 2.2.2. University of Maryland's Cessna 402B Research Aircraft

215 The UMD operated a Cessna 402B research aircraft equipped with an instrument package
216 to measure gaseous and particle pollutants [*He et al.*, 2014, 2016]. Separate inlets for gases and

particles, as well as temperature and humidity sensors were installed at the nose of the aircraft. Temperature, humidity, and pressure were measured using a Vaisala probe (Model PTU300, Vaisala Inc., Woburn, MA). Flight tracks were recorded using a handheld GPS and an aircraft INS. Horizontal two-dimensional wind speed was calculated by a Garmin G600 system using information from an INS, GPS, and an air data computer (Model GTN650, Garmin, Chicago, IL). The UMD Cessna research aircraft was equipped with a suite of trace gas and aerosol analyzers. Those relevant to this study include a Picarro G2401-m CRDS for 0.5 Hz CO_2, CH_4, CO and H_2O_v measurements, and an LGR OA-ICOS for 1 Hz NO_2 measurements [*Brent et al.*, 2015].

For the flights in D.C.-Balt, the UMD Picarro CRDS was calibrated both on the ground and in the air with analytical standards from NIST. The Picarro G2401-m instrument has measured precisions of 0.02 ppm for CO_2, 0.2 ppb for CH_4, and 4 ppb for CO (standard deviations (1σ) of 0.5 Hz data over five minutes) for atmospherically relevant trace species mole fractions measured from dry analytical standards. The manufacturer-reported H_2O_v precision is 1 $\times 10^{-2}$ mmol mol^{-1} for humid air samples.

2.3. Mass Balance Flight Design

Airborne mass balance experiments were performed with the Purdue and the UMD aircraft to quantify citywide GHG emissions from Indianapolis and D.C.-Balt [*Trainer et al.,* 1995; *Kalthoff et al.,* 2002; *Mays et al.,* 2009; *Karion et al.,* 2013, 2015*; Gioli et al.,* 2014; *O'Shea et al.,* 2014; *Petron, et al.,* 2014; *Cambaliza et al.,* 2014, 2015; *Lavoie, et al.,* 2015; *Heimburger et al.,* 2017]. Alternative airborne methods for estimating urban fluxes of energy, greenhouse gases, and other anthropogenic pollutants have been reported [*Font et al.,* 2015; *Karl et al.,* 2009; *Trousdell et al*., 2016; *Vaughan et al.,* 2016]. In an airborne mass balance experiment, transects are flown upwind and downwind of an emission source, D.C.-Balt or Indianapolis, and the emission rate of the species of interest, H_2O_v, is calculated from the urban enhancement in mole fraction relative to background and the perpendicular component of the wind speed relative to the flight track. Figure 1a-b shows the ALAR's flight path and altitude, respectively, during the 27 February 2015 D.C.-Balt mass balance flight. The 27 February 2015

246 flight is used throughout the paper as a representative example of an urban mass balance flight
247 for which an urban H_2O_v excess signal is observed. Flight paths from the remaining mass balance
248 flights are provided in Figure S2. All flights commenced at approximately noon to minimize
249 atmospheric boundary layer growth throughout the duration of the flight [*Stull,* 1988], consistent
250 with our observations. Typically, a vertical profile was flown on the upwind side of the city to
251 characterize the atmospheric boundary layer, followed by an upwind transect to measure the
252 H_2O_v mole fraction entering the study area. Next, downwind transects were flown at different
253 altitudes approximately equally spaced throughout the boundary layer, (Figure 1b). Downwind
254 transects were conducted approximately 30 km and 70 km from the center of Indianapolis and
255 D.C.-Balt, respectively. Downwind transect locations are chosen so that emissions have time to
256 mix through the boundary layer. While this results in a lower uncertainty in the calculated
257 results, our analysis makes no assumptions about a well-mixed boundary layer. The locations of
258 D.C.-Balt downwind transects were also in part dictated by flight restrictions. The number of
259 downwind transects completed in each flight was dependent on city size and the time available
260 before the atmospheric boundary layer became stable. The downwind transects were designed to
261 extend several tens of kilometers beyond the horizontal bounds of the urban area to ensure
262 complete sampling of the urban plume, and appropriate sampling of background H_2O_v mole
263 fractions at the lateral edges of the downwind transects. For most flights, a second vertical
264 profile was flown downwind of the city to determine boundary layer depth evolution, as well as
265 characterize vertical mixing downwind of the metropolitan area.

266

267 2.4. Background Determination

268 One of the objectives of this study is to determine urban emission rates of H_2O_v *in excess*
269 of the surrounding rural area. A background concentration serves as a reference for determining
270 the incremental urban enhancement in H_2O_v mole fraction, and is ideally representative of air not
271 influenced by the urban area, but of the same air mass as the air sampled downwind of the urban
272 center. To determine the incremental urban enhancement in H_2O_v relative to the surrounding
273 rural areas, background H_2O_v mole fractions were defined from air sampled along the lateral
274 edges of the downwind transects where mole fractions are relatively constant, and are likely a

result of rural influence only. This approach has been used in aircraft mass balance experiments to quantify CH_4 and CO_2 emissions from cities and natural gas fields [*Cambaliza et al.,* 2014, 2015; *Karion et al.,* 2015; *Heimburger et al.,* 2017]. Measurements of H_2O_v mole fraction made along upwind transects were used to identify spatial variability in H_2O_v mole fraction entering the study areas.

Figure 2 shows the urban H_2O_v plume intercepted downwind of D.C.-Balt on 27 February 2015 (plume profiles from the remaining flight days are shown in Figure S2). A line (cyan in Figure 2) connecting the baseline H_2O_v mole fractions at either ends of the transects defines the background mole fraction at each data point sampled along the urban plume. Downwind transects were flown well past the boundaries of the urban area, so that air sampled near transect ends did not pass over urbanized areas, and were thus representative of background (rural) mole fractions at the time and location the downwind transect was flown. We define the transition from rural-influenced air to urban-influenced air as the location that the downwind H_2O_v mole fractions are greater than the background mole fraction plus three times the standard deviation of the background. The standard deviation in H_2O_v mole fraction along the upwind transect is used as a proxy for defining the standard deviation of the background, assuming that variability in H_2O_v mole fraction along the upwind transect would be similar to the variability in downwind H_2O_v mole fraction not influenced by the urban area. This criterion (background plus three standard deviations of the background) is also used for determining if an urban H_2O_v excess signal exists (as indicated in Table S1).

H_2O_v mole fractions observed upwind of the urban areas (red trace in Figure 2) were often similar in magnitude to the linear, transect-edge-defined background (cyan trace in Figure 2). Instances when transect-edge-defined background H_2O_v mole fractions were higher or lower relative to upwind mole fractions could indicate that the surrounding rural area acted as a source of moisture or there was entrainment of drier free tropospheric air, respectively. We have previously determined that upwind transects do not provide a reliable background measurement for mass balance experiments, but rather, that the rural edges of the downwind transects provide a more reliable background, in part because the measurements on the transect edges are conducted closer in time to urban plume sampling [*Cambaliza et al.,* 2014, *Karion et al.,* 2015, *Heimburger et al*., 2017]. Measurements of background mole fraction for all flights when an

urban H_2O_v excess signal was observed are explained in detail in the captions of Figure S2.1-7 in the Supporting Information (SI).

2.5. Emission Rate Calculation

To quantify the emission rate of urban H_2O_v excess from D.C.-Balt and Indianapolis, the flux, $F_{Urban,ij}$, of urban H_2O_v excess is calculated at each downwind data point (unique distance along the downwind track (i) and altitude (j)), according to Equation 1.

$$F_{Urban,ij} = U_{\perp,ij} \cdot (H_2O_{v_{dw,ij}} - H_2O_{v_{bg,ij}}) \quad (1)$$

For Equation 1, reported H_2O_v mole fractions have been converted to molar density (mol m^{-3}) using the ideal gas law, and simultaneous pressure and temperature measurements (an expanded form of Equation 1 is in the SI). The background mole fraction (Section 2.4), $H_2O_{v_{bg,ij}}$, is subtracted from the corresponding downwind H_2O_v mole fraction, $H_2O_{v_{dw,ij}}$, giving an urban enhancement in H_2O_v. The H_2O_v enhancement is multiplied by the perpendicular component of the wind speed (50 Hz winds averaged over 10 seconds), $U_{\perp,ij}$ (m s^{-1}). The result is an urban H_2O_v excess flux (mol m^{-2} s^{-1}), $F_{Urban,ij}$, calculated at each data point sampled downwind of the urban center as shown in Figure 3.

To determine the percent contribution of urban-derived H_2O_v to the total transport (background + urban excess) of atmospheric boundary layer H_2O_v exiting the urban area, the total H_2O_v flux, $F_{Total,ij}$, at any point is calculated according to Equation 2. Equation 2 is identical to Equation 1, except that a background mole fraction, $H_2O_{v_{bg,ij}}$, is not subtracted from the downwind H_2O_v mole fractions, $H_2O_{v_{dw,ij}}$.

$$F_{Total,ij} = U_{\perp,ij} \cdot H_2O_{v_{dw,ij}} \quad (2)$$

The flux values defined at each downwind point, $F_{Urban,ij}$ and $F_{Total,ij}$, are used as inputs to a kriging program (MATLAB EasyKrig3.0) to interpolate/extrapolate a two-dimensional x-z plane, or matrix, of downwind H_2O_v fluxes, M_{Urban} or M_{Total} [*Mays et al.,* 2009; *Cambaliza et al.,* 2014, 2015]. The flux matrices are gridded at a resolution of 100 m (x

dimension) x 10 m (z dimension), from the surface to the top of the boundary layer. We define boundary layer depth (z_i) as the altitude along the vertical profile associated with the greatest change in potential temperature (maximum $d\theta/dz$, where θ is potential temperature) [*Cambaliza et al.,* 2014]. Vertical profiles with indicated boundary layer height for each day are provided in the SI. The citywide H_2O_v emission rate, ER_{Urban} (mol s^{-1}; reported in units of kg s^{-1}), is calculated by integrating the urban H_2O_v excess flux matrix, M_{Urban}, across the horizontal bounds of the city, and vertically from the surface to the top of the boundary layer (z_i) according to Equation 3:

$$ER_{Urban\ or\ Total} = \int_0^{z_i} \int_{-x}^{+x} M_{Urban\ or\ Total}\, dx\, dz \quad (3)$$

Similarly, the total H_2O_v transport emission rate (ER_{Total}) is calculated according to Equation 3 by integrating over the total H_2O_v flux matrix, M_{Total}. In principle, the uncertainty in the ratio of urban H_2O_v excess to the total H_2O_v transport through the study area (ER_{Urban}: ER_{Total}) would be smaller than the uncertainty of the individual emission rates because the wind speed and kriging uncertainties would be effectively canceled. An uncertainty analysis of the mass balance emission rate calculation is provided in the SI.

3. Results and Discussion

3.1. Urban H_2O_v Enhancements and Emission Rates

An elevated urban H_2O_v signal was observed on five (13 February, 20 February, 27 February, 9 March, and 12 March 2015) of the eight flights conducted around D.C.-Balt. An urban H_2O_v excess signal was not observed on 19 February, 23 February, or 25 February 2015 in D.C.-Balt. Figure S4 shows flight paths and observations of upwind and downwind H_2O_v mole fractions for these days. Between March 2011 to December 2014, an urban H_2O_v excess signal was observed on two of 16 mass balance flights conducted in Indianapolis during non-growing season months (November through March).

The magnitude of the urban H_2O_v signal varied by day and, for some flights, by altitude depending on the extent of vertical mixing within the boundary layer. The boundary layer downwind of D.C.-Balt was poorly mixed on 27 February 2015 as the magnitude of the H_2O_v, CO_2, CH_4, NO_2, and aerosol plumes are altitude dependent (Figure 2; Figure 4a-e). The highest downwind transect conducted on 27 February 2015 is shorter than the lower two downwind transects (Figure 2-4) because the aircraft had to stop to refuel. Data collected after refueling (Figure 1b) on 27 February 2015 is not used in our analysis because large variability in H_2O_v and other GHG mole fractions was observed along the remainder of the final downwind transect. This variability is characteristic of mixed layer decay observed in late afternoon or early evening [*Acevedo and Fitzjarrald,* 2001; *Lothon et al.,* 2014].The maximum urban enhancement in H_2O_v mole fraction, 1.5 mmol mol^{-1}, was observed on the lowest downwind transect (390 m above sea level (msl)) of the 27 February 2015 flight. The maximum enhancement in H_2O_v mole fraction ranged between 0.24 mmol mol^{-1} – 1.5 mmol mol^{-1} for the five D.C.-Balt flights. An urban H_2O_v excess signal of 0.72 mmol $mol^{-1}$and 0.65 mmol mol^{-1} was observed on two mass balance flights conducted in Indianapolis on 8 November 2012 and 25 November 2014, respectively. Both the presence and magnitude of the urban H_2O_v excess signals in D.C.-Balt and Indianapolis exhibited inter-day variability, and were not necessarily proportional to city size (e.g. the observed Indianapolis H_2O_v excess signals were sometimes greater than the D.C.-Balt signals). Maximum urban H_2O_v enhancements for the D.C.-Balt and Indianapolis flights can be found in Table 1.

Urban emission rates, calculated according to Equations 1 and 3, ranged from 1.6 (±0.66) $\times 10^4$ – 1.7 (±0.81) $\times 10^5$ kg H_2O_v s^{-1} for D.C.-Balt and 2.1 (±1.2) $\times 10^4$ – 3.5 (±1.4) $\times 10^4$ kg

H_2O_v s^{-1} for Indianapolis. Urban H_2O_v excess emission rates are reported in Table 1. Uncertainties associated with the calculation of citywide emission rates were estimated on average to be 46% (1σ; range: 39% - 59%), and are discussed in the SI. The percent contribution of urban H_2O_v excess to the total flow (background + urban excess; discussed in Methods Section 2.5) of atmospheric boundary layer H_2O_v out of the study areas range from 1.5 – 8.4% (average: 4.1%) for the D.C.-Balt flights, and average 2.8% for the Indianapolis flights (Table 1).

It is important to note that this range of emission rates is not representative of every mass balance flight flown around the D.C.-Balt and Indianapolis areas, rather the range corresponds only to days when an urban H_2O_v excess was observed. Our observations of urban H_2O_v excess occurred during winter, when transpiration rates and saturation vapor pressure are lower than in summer months. During this time period, urban H_2O_v excess signals may be easier to observe relative to the noise, or natural variability in H_2O_v mole fractions. There were three of eight D.C.-Balt flight days and 14 of 16 Indianapolis mass balance flights on which the downwind H_2O_v mole fractions were approximately equal to, or less than, the observed upwind H_2O_v mole fractions. Sisterson and Dirks [1978] measured lower specific humidity values along airborne transects downwind of St. Louis, Missouri in summertime, relative to upwind transects. Sisterson and Dirks [1978] hypothesize decreased rates of evapotranspiration within the city and UHI-induced entrainment contributed to lower downwind specific humidity.

3.2. Spatial Correlation with Anthropogenic Pollutants

Figure 4a-e shows that the plume shapes and widths of the other anthropogenic species, CO_2, CH_4, NO_2, and aerosol number concentration, respectively, track the urban H_2O_v plume. Periods without NO_2 data in Figure 4d correspond to times the analyzer was performing five-minute-long internal zeroes (every 30 minutes of sampling). Similar urban plume shapes of H_2O_v and other anthropogenic species were observed during the other D.C.-Balt flights (Figure S2.3-7). Additionally, the most intense H_2O_v peak observed downwind of the D.C.-Balt area on 27 February 2015 is co-located with the urban aerosol plume and the greatest aerosol concentrations as shown in Figure 4f-g. Aerosol number concentration increased three to fourfold after passing over D.C.-Balt, with little growth observed in aerosol diameter (Figure 4f-g). Hygroscopic aerosol with diameters greater than ~0.1 μm can act as CCN, and elevated aerosol concentrations can produce smaller and more numerous droplets that take longer to grow to precipitation size

droplets under constant moisture conditions, impacting cloud optical properties and precipitation yield and frequency [*Kreidenweis et al.,* 2005; *Bréon,* 2006]. However, if aerosol emissions are collocated with H_2O_v emissions, as indicated by the present observations (Figure 4a, e-g), moisture conditions would not be constant, and may counteract aerosol-delayed precipitation [*Rosenfeld et al.,* 2008]. Indeed, it has also been shown that H_2O_v can have a stronger impact on cloud cover than aerosol optical depth [*Kourtidis et al.,* 2015].

The downwind enhancements of the combustion products CO_2, H_2O_v, and NO_2 were atmospherically correlated (Pearson correlation coefficient of 0.83 for CO_2 and H_2O_v) during the 27 February 2015 flight (Figure 5). This correlation was also observed for three of the other D.C.-Balt flights, but to a lesser extent ($r = 0.41 – 0.50$). There was one D.C.-Balt flight day, 9 March 2015, where no correlation ($r = 0.1$) was observed. Figure S5 shows correlation plots of combustion product enhancements for the remaining D.C.-Balt flight days when an urban H_2O_v excess signal was observed. This implies that the urban H_2O_v excess is frequently associated spatially and temporally with anthropogenic activities within D.C.-Balt. While the observed urban plumes of H_2O_v, CO_2, CH_4, NO_2, and aerosol track a similar shape (Figure 4a-e) on 27 February 2015 in D.C.-Balt, and H_2O_v, CO_2, and NO_2 enhancements show correlation of varying strengths (Figure 5, S5) data from the Indianapolis flights do not always suggest an equally strong spatial correlation between these species. Figure 6a-c shows urban plume profiles of H_2O_v, CO_2, and CH_4, respectively, from the 8 November 2012 flight in Indianapolis (flight path shown in Figure S2.1a). The urban H_2O_v plume was observed to be slightly broader, and did not exhibit the same double peak profile of the CO_2 and CH_4 plumes during the 8 November 2012 flight. Similarly, the H_2O_v plume observed on the 25 November 2014 flight is offset to the south of the CH_4 and CO_2 plumes (Figure 6d-f, respectively; flight path shown in Figure S2.2a). In the case of the observations from 25 November 2014, it appears that the urban H_2O_v plume is originating from the southern outskirts of Indianapolis, which is primarily suburban. The largest CO_2 and CH_4 plumes appear to originate slightly south of central Indianapolis, likely as a result of emissions from the city's power plant and landfill, which are located in the southwest part of the city. Potential reasons for differences in observed spatial relationships between these atmospheric species of urban origin are discussed in Section 3.3.3.

437

438 3.3. Sources and Impacts of Urban H_2O_v Excess

439 Below we discuss sources and conditions likely contributing to the enhancement in H_2O_v
440 mole fractions observed downwind of the D.C.-Balt and Indianapolis areas, including direct
441 anthropogenic moisture sources such as combustion and evaporative cooling, moisture
442 contributions from local bodies of water, which we believe to be negligible, and finally,
443 differences in urban and rural evaporation rates. Lastly, we consider the radiative impact of
444 elevated H_2O_v and GHG mole fractions on the urban boundary layer, more specifically UHI
445 intensity.

446

447 3.3.1. Direct Anthropogenic Sources

448 Combustion sources have been identified as a major wintertime contributor to urban
449 moisture in mid-latitude cities, contributing up to 13% of surface-level moisture during inversion
450 periods in Salt Lake City, UT, and causing urban low-temperature fog in Edmonton, Alberta,
451 Canada [*Hage,* 1972, 1975; *Ackerman,* 1987; *Gorski et al.,* 2015]. To estimate the contribution
452 of H_2O_v from combustion sources, CO_2 emission rates calculated according to the procedure
453 described in the Methods Sections 2.4-5, were multiplied by a H_2O_v:CO_2 combustion ratio
454 weighted for the fossil fuel use distribution in the D.C.-Balt area [*EPA,* 2015; *EIA,* 2015]. The
455 calculation of the consumption-weighted H_2O_v:CO_2 combustion ratio, estimated to be
456 approximately 1.2 H_2O:1 CO_2, is discussed in the SI. Heating and electricity generation via fossil
457 fuel combustion (electricity generation from nuclear power is also significant in the area) in the
458 D.C.-Balt study area is mainly achieved through the burning of coal and natural gas. Petroleum is
459 rarely used for heating or electricity generation in the area, and is mainly consumed by the
460 transportation sector after it has been processed into gasoline [*EIA,* 2016a]. The magnitude of the
461 combustion-derived H_2O_v emission rates, presented as $ER_{Combustion}$ in Table 2, appear to be
462 inversely proportional to temperature, as we expect in the winter due to increased fossil fuel
463 consumption for space-heating. Also presented in Table 2 is the contribution of combustion-
464 derived H_2O_v to the urban H_2O_v excess signal, which was estimated to range from 1.0-9.6%.
465 However, the maximum contribution of combustion-derived H_2O_v to the total flow of H_2O_v

exiting the study area is negligible, with a maximum contribution of ~0.32%. Similar to our analysis, Kalanda et al. [1980] report high urban latent heat fluxes, but estimate the maximum combustion-derived H_2O_v contribution to be at least an order of magnitude lower than the observed latent heat fluxes. Given our combustion-derived H_2O_v estimates, it is likely that the observed correlation between combustion products CO_2, H_2O_v, and NO_2 shown in Figure 5 (and Figure S5a,b,d) represents spatial coherence between combustion sources and the sources of urban-derived H_2O_v in D.C.-Balt on some days. The observed combustion product correlation on 9 March 2015 (Figure S5c) does not show as strong a relationship as the other D.C.-Balt days. Additionally, the plume shapes of H_2O_v and CO_2 from Indianapolis in Figure 6 do not track one another, indicating that combustion sources are not the dominant source of urban H_2O_v excess for these days.

In addition to the H_2O_v produced from combustion reactions, the other main form of direct anthropogenic moisture is from the phase change associated with evaporative cooling equipment [*Sailor,* 2011]. Evaporative cooling from air conditioning systems was implicated as the major contributor to large summertime latent heat fluxes in Tokyo, Japan by Moriwaki et al. [2008]. However, the authors report winter urban latent heat fluxes to be nearly two orders of magnitude lower than their summer estimates. Evaporative cooling towers from energy generating stations are sources of direct anthropogenic moisture throughout the year. Latent heat flux contributions from cooling towers are often not included in urban energy balance modeling because there are few quantitative reports on their contribution, and these estimates tend to be small [*Grimmond et al.,* 2010]. Cooling tower plume dispersion models have been evaluated with empirical data collected by the EPA and United States national labs during the 1970s [*Meroney,* 2006; *Ruiz et al.,* 2013]. Stockham [1971] reports periodic H_2O_v emissions over a four-month period from the cooling towers of a coal-fired 1,800 MW electricity generation facility. From the data reported by Stockham [1971], the linear relationship ($R^2 = 0.983$, N=11) between the cooling tower H_2O_v emission rate and the capacity at which the facility was operating was determined to be 4.1 g H_2O_v s^{-1} MW^{-1} for every percent of operating capacity. Orville et al. [1981] simulated emissions to be 2.5×10^4 kg H_2O_v s^{-1} from a 48,000 MW power park using an unspecified fuel source. Hane [1978] simulated slightly higher emissions, 3×10^4 kg H_2O_v s^{-1}, from a nuclear plant, but did not specify the plant's power output. The power plants within the D.C.-Balt study area were capable of collectively generating ~15,700 MW of power

497 during Winter 2015, and the primary fuel source was coal for most of the facilities [*EIA,* 2016b].
498 By applying the operating capacity-emission rate relationship observed by Stockham [1971] to
499 the D.C.-Balt electricity generating facilities, we estimate the cooling towers within the study
500 area would emit ~6.5×10^3 kg H_2O_v s^{-1} if operating at full capacity. Similarly, scaling Orville et
501 al. [1981]'s emissions by power output for the D.C.-Balt facilities results in a maximum
502 emission rate of 8.2×10^3 kg H_2O_v s^{-1}. Averaging the cooling tower emission estimates based on
503 Stockham [1971] and Orville et al. [1981] gives a maximum collective cooling tower emission
504 rate of 7.4×10^3 kg H_2O_v s^{-1} for D.C.-Balt. Repeating this calculation for the energy generating
505 facilities' cumulative power output of 1,400 MW in Indianapolis, gives a maximum cooling
506 tower emission rate of 6.7×10^2 kg H_2O_v s^{-1}. Given these operating conditions, cooling tower
507 H_2O_v emissions could contribute up to ~43% of the urban excess H_2O_v signal for the D.C.-Balt
508 flight day with the smallest observed emission rate, 1.60×10^4 kg s^{-1} on 13 February 2015.
509 However, assuming the same operating conditions, cooling tower H_2O_v emissions would only
510 contribute ~4% to the maximum observed urban excess H_2O_v emission rate of 1.68×10^5 kg s^{-1}
511 on 27 February 2015 in D.C.-Balt. Similarly, cooling tower emissions from energy generating
512 facilities operating at full capacity in Indianapolis would only contribute approximately 3% and
513 2% to the urban H_2O_v excess signal observed on 8 November 2012 and 25 November 2014,
514 respectively. Maximum cooling tower emission rate estimates and their contribution to the
515 observed urban H_2O_v excess signals are provided in Table 2.

516

3.3.2. Contribution from Local Bodies of Water

Due to the proximity of the D.C.-Balt area to the Atlantic Ocean, it is possible that moist air parcels originating from the sea-breeze were sampled aloft on their return circulation toward the ocean [*Stull,* 1988]. However, moist sea-breeze air would likely contribute to humidity levels equally along the coast, and not contribute preferentially to urban air than rural air. A sea-breeze circulation was not observed on 27 February 2015, as the wind direction measured along the lowest (390 msl) downwind transect originated from the northwest (Figure S6), nor was it observed during the other D.C.-Balt flight days.

The Chesapeake Bay, across which downwind transects were sometimes flown, was frozen for the majority of the WINTER field campaign (Figure S7). We note that the vapor pressure of ice is only slightly lower than that of liquid water at the same temperature. We believe it is unlikely that there was a significant contribution of moisture from the Chesapeake Bay considering the well-defined H_2O_v plumes intercepted directly downwind of the D.C.-Balt area (Figure 1a; Figure S2.3-7), rather than broad plumes spanning the length of the Chesapeake Bay as would be expected if the Chesapeake was the excess H_2O_v source. The most intense plume of excess H_2O_v observed on 27 February 2015 was in fact upwind of the Chesapeake Bay (Figure 1a). We note again that the urban H_2O_v excess signal is often correlated temporally and spatially with anthropogenic activities, as demonstrated by the combustion product correlation plots for most of the flights in D.C.-Balt (Figure 5; Figure S5). Additionally, an urban H_2O_v excess signal has been observed downwind of Indianapolis (Figure 6; Figures S2.1-2), in the absence of significant bodies of water. Relative to D.C.-Balt, Indianapolis is a meteorologically simple environment, and the nearest body of water, Lake Michigan, is over 200 km north of the city.

3.3.3. Urban-Rural Energy Balance Differences

Our estimates indicate that the combined emissions from combustion sources and cooling towers at most account for approximately half of the observed enhancement in H_2O_v mole fractions in the outflow from D.C.-Balt and Indianapolis. Additionally, we infer from our observations that nearby bodies of water did not contribute to the observed H_2O_v enhancement in

546 the D.C.-Balt or Indianapolis outflows. Additional sources of urban-derived H_2O_v must have
547 contributed to the enhancement in urban H_2O_v outflow on the days when an elevated urban H_2O_v
548 signal was observed. High latent heat fluxes have been reported within urban areas, particularly
549 following precipitation events, by several urban energy balance studies [*Oke,* 1979; *Kalanda et*
550 *al.,* 1980; *Oke and McCaughey,* 1983; *Grimmond,* 1992; *Oke et al.,* 1992; *Offerle et al.,* 2006;
551 *Ward et al.,* 2013; *Ramamurthy et al.,* 2014; *Ao et al.,* 2016]. Rapid urban evaporation, providing
552 there is available moisture, can result from the oasis effect, a local or microscale advection
553 process that occurs when warmer or drier air is advected from above an impervious surface to a
554 moist and/or porous surface creating a large moisture gradient, initiating faster rates of
555 evaporation and snowmelt [*Oke,* 1979; *Bengtsson and Westerström,* 1992; *Neumann and Marsh,*
556 1998; *Moriwaki and Kanda,* 2004]. The northeastern United States received significant amounts
557 of snow and rain throughout the WINTER campaign. Over the one month of Purdue and UMD
558 mass balance flights (13 February to 12 March 2015), the D.C.-Balt area received approximately
559 101 mm of precipitation (reported by Washington National and Baltimore-Washington
560 International Airports). From 1 January to 12 March 2015 (date of last D.C.-Balt mass balance
561 flight), the D.C.-Balt area received approximately 29 mm more precipitation than average (snow
562 accumulation is converted to snow water equivalent). The oasis effect could be a contributor to
563 the observed urban H_2O_v exces signals. We note that our observations indicate that prior
564 precipitation does not necessarily lead to an observable urban H_2O_v excess signal. Similar
565 amounts of snow fell in D.C.-Balt prior to all flight days, including days when an urban H_2O_v
566 excess signal was not observed (Table S1). While our measurements do not allow us to comment
567 on the conditions impacting urban evaporation rates, other studies have shown that wintertime
568 urban latent heat fluxes are sensitive to the physical state and availability of water on and within
569 impervious and natural land cover [*Offerle et al.,* 2006; *Lemonsu et al.,* 2008; *Leroyer et al.,*
570 2010; *Bergeron and Strachan,* 2012].

571 In addition to being influenced by micro- and local scale advection processes, rates of
572 evaporation and urban snowmelt can be influenced by large anthropogenic sensible heat fluxes in
573 areas where space-heating occurs [*Bengtsson and Westerström,* 1992; *Grimmond,* 1992; *Sailor,*
574 2011; *Bergeron and Strachan*, 2012]. It is possible that anthropogenic heat fluxes during the
575 D.C.-Balt flights were significant considering the sub-zero temperatures (Table 2) and space
576 heating that would be required. Urban snowmelt has also been shown to be influenced by

longwave radiation emitted from buildings with high emissivity values, and the relatively lower albedo of the surrounding urban surfaces [*Lemonsu et al.,* 2008; *Leroyer et al.,* 2010; *Bergeron and Strachan,* 2012]. Urban snow typically is cleared from parking lots, roads, and sidewalks and gathered in large piles [*Järvi et al.,* 2014], where it can become packed and mixed with gravel and dirt, significantly lowering its albedo [*Bengtsson and Westerström,* 1992; *Ho and Valeo,* 2005]. The effect of road salt on evaporation within cities is complex. Road salt helps to melt ice and snow on roadways by decreasing the freezing point of water, but the resulting salt-meltwater solution has a vapor pressure lower than that of pure water.

At present, our measurements cannot explain why the urban H_2O_v excess signal is observed on some days, but not others. Our estimates indicate that combustion and cooling tower emissions cannot entirely account for the magnitude of the observed urban H_2O_v signals. Indeed, if combustion and cooling tower emissions were dominant sources, we would expect elevated urban H_2O_v mole fractions to be observed on every flight. But this is not the case for the D.C.-Balt flight days on 19, 23, and 25 February 2015 when an elevated urban H_2O_v signal was not observed (Figure S4). If enhanced urban snowmelt and evaporation is widespread, i.e. on the city-scale, it could be a dominant urban H_2O_v excess source. It is likely that some combination of abundant moisture, anthropogenic heat flux, radiative properties of urban surfaces, and local-scale advection processes resulted in the urban areas acting as sources of indirect anthropogenic H_2O_v. Enhanced rates of urban evaporation and snowmelt could be responsible for the sometimes spatially offset urban H_2O_v plume relative to the plumes of other GHGs (Figure 6 and Figure S5c). For example, emissions of CO_2 and CH_4 from power plants, transportation, natural gas distribution networks, and landfills are concentrated at the center of Indianapolis [*Cambaliza et al.,* 2014], but significant advection-assisted evaporation could occur along the highways and residential areas surrounding the urban center. Bergeron and Strachan [2012] report different wintertime H_2O_v emission responses from urban and suburban tower sites within 18 km of one another in Montreal. Our measurements allow for city-wide estimates of urban H_2O_v excess emissions relative to rural areas. To determine if rapid evaporation and snowmelt is a dominant contributor to the urban H_2O_v excess signal on the city-scale, future studies should conduct mobile measurements of urban-rural humidity differences [*Chandler,* 1967; *Kopec,* 1973; *Bornstein and Tam,* 1977; *Sisterson and Dirks,* 1978; *Richards,* 2005] simultaneously with local-

scale measurements of snowmelt/evaporation and energy balance within and outside the urban area.

3.3.4. Impacts of Elevated H_2O_v on the Urban Heat Island

Radiative forcing by anthropogenic GHG emissions is often considered in terms of global temperature increase. But the question remains as to whether the combined effects of elevated CO_2, CH_4, and H_2O_v can impact the intensity of the daytime UHI. On average, the air advected out of the D.C.-Balt area was elevated in CO_2, CH_4, and H_2O_v, by 4 ppm, 26 ppb, and 0.43 mmol mol^{-1}, respectively, on days when an urban H_2O_v excess signal was observed. Past studies have considered the impact of elevated urban GHG mole fractions on UHI intensity [*Oke et al.,* 1991; *Holmer and Eliasson,* 1999; *McCarthy et al.,* 2010]. For some of these studies, H_2O_v [*Holmer and Eliasson*, 1999] or CO_2 [*McCarthy et al*., 2010] were considered individually, or the focus was on simulating the nighttime UHI [*Oke et al.,* 1991; *Holmer and Eliasson,* 1999].

The impact of enhanced urban GHG mole fractions on UHI intensity was assessed through idealized experiments using the Rapid Radiative Transfer Model (RRTM; methods discussed in the SI). Our calculations from RRTM show that on all five days the urban enhancement in CO_2 and CH_4 mole fractions had a negligible impact on the longwave radiation budget. McCarthy et al. [2010] show that the UHI intensity of megacities are positively influenced in the hypothetical scenario of increasing the global atmospheric CO_2 mole fraction to 645 ppm. Their analysis, however, is extreme in comparison to our simulation of the relative impact, which used the average observed urban enhancement in CO_2 mole fraction, 4 ppm, for a total of 412 ppm CO_2 well-mixed throughout the D.C.-Balt boundary layer. Enhanced H_2O_v had a larger, but still minimal, impact on the longwave radiation budget than CO_2 and CH_4. Relative to the control scenario, elevated H_2O_v mole fractions produced a cooling of roughly $-0.1^oC\ day^{-1}$ at the top of the boundary layer, and a comparable warming of $0.1^oC\ day^{-1}$ at the surface (Figure S8). These values are small, but could contribute to the average afternoon UHI of ~1.5^oC observed in Washington, D.C. in winter by 6-7% at the surface [*Hicks et al.,* 2010]. Absorption of shortwave radiation (warming) by H_2O_v during the daytime is less in magnitude than longwave cooling, thus producing a net cooling within the boundary layer during the day that is less than $-0.1^oC\ day^{-1}$. Holmer and Eliasson [1999] also report competing impacts from elevated urban humidity on UHI intensity, which result in a net cooling effect. The small GHG-induced

637 radiative impacts in the urban plume suggested by these calculations are consistent with results
638 from previous studies [*Oke et al.,* 1991; *Holmer and Eliasson,* 1999].

639

4. Conclusions

Our wintertime airborne case studies around D.C.-Balt and Indianapolis reveal instances of significant urban emissions of H_2O_v that result in H_2O_v mole fractions downwind of the urban area to be in excess of rural H_2O_v mole fractions. On flight days when an elevated H_2O_v signal was observed, the emission rate of excess urban H_2O_v ranged between 1.6 (±0.66) × 10^4 – 1.7 (±0.81) × 10^5 and 2.1 (±1.2) × 10^4 – 3.5 (±1.4) × 10^4 kg s^{-1} for D.C.-Balt and Indianapolis, respectively. The emissions of excess urban H_2O_v contributed between 1.5-8.4% to the total flow of atmospheric boundary layer H_2O_v out of the urban areas. Our observations of urban H_2O_v excess occurred during times of the year when transpiration rates were likely very low. Furthermore, because of the low temperatures associated with winter, saturation vapor pressure is lower than in summer months, and urban H_2O_v excess signals are easier to observe relative to the noise, or natural variability in H_2O_v mole fractions.

To our knowledge this is the first study to report elevated H_2O_v mole fractions downwind of an urban area using airborne platforms during daytime, and which has shown city-wide H_2O_v excess, rather than local scale observations. Previous urban-rural humidity studies employed mobile [*Chandler,* 1967; *Kopec,* 1973; *Richards,* 2005] and airborne platforms [*Bornstein and Tam,* 1977; *Sisterson and Dirks,* 1978] to traverse larger rural and urban areas, but none reported elevated moisture levels downwind of cities during midday. Studies of urban-rural humidity gradients and energy balance studies typically employ meteorological and eddy covariance towers, where the locations of rural stations are purposely chosen so that they are not influenced by a nearby urban center. Urban areas are heterogeneous, and thus tower location would be very important.

A combination of sources and conditions was likely responsible for the observed urban H_2O_v signal reported here. Using CO_2 emissions estimates and a combustion fuel consumption-weighted H_2O_v:CO_2 ratio, it was estimated that combustion sources contributed a maximum of 9.6% to the elevated urban H_2O_v signal, and only contributed a maximum of 0.32% of the total transport of boundary layer H_2O_v through the study areas. We have shown that contributions from evaporative cooling towers when energy generation facilities are operating at maximum capacities could account for approximately 2% to 43% of the observed urban H_2O_v excess signals. A dominant source contributing to the urban H_2O_v signal could be rapid urban snowmelt

and evaporation either from increased wintertime anthropogenic heat flux and/or advection-assisted evaporation. We note that prior precipitation events do not necessarily lead to observable urban H_2O_v signals. Combining mobile city-scale H_2O_v measurements with micro- and local-scale measurements of snowmelt, evaporation, and energy fluxes at several rural and urban sites could be a next step in directly determining the relative contribution of these processes to the urban H_2O_v excess signal.

We quantified the impact of GHG radiative forcing on the intensity of the UHI using RRTM, and found that elevated urban mole fractions of H_2O_v, CO_2, and CH_4 individually, and collectively, had small impacts on UHI intensity. At the surface, elevated urban mole fractions of H_2O_v could be responsible for 6-7% of UHI intensity. However, this surface warming is counteracted by longwave cooling at the top of the boundary layer. Atmospheric boundary layer effects caused by urban H_2O_v emissions could be significant, and include urban area-modified downwind cloud cover and weather [*Mölders and Olson,* 2004; *Rosenfeld et al.,* 2008; *Trusilova et al.,* 2008; *Twohy et al.,* 2009; *Kourtidis et al.,* 2015]. In addition, recent findings indicate that aerosol chemistry and optical properties could be modified in the downwind region of the urban environment [*Twohy et al.,* 2009; *Carlton and Turpin,* 2013; *Hodas et al.,* 2014; *Guo et al.,* 2015; *Rindelaub et al.,* 2015].

Acknowledgments and Data

We thank Joel A. Thornton and Steven S. Brown for organizing and inviting us to take part in the WINTER campaign. We are grateful for help with the design, installation, and maintenance of the ALAR instrument package we received from Purdue University's Jonathan Amy Facility for Chemical Instrumentation. We thank Daniel P. Sarmiento for reading and suggesting improvements to this manuscript. We acknowledge support for this research from James Whetstone and the National Institute of Standards and Technology (NIST), for which we are grateful. We also thank three anonymous reviewers for valuable input on this manuscript. The UMD and Purdue flight experiments and analysis were supported by NIST Award 70NANB14H333 and 70NANB14H332, respectively. The radiative transfer modeling was supported by the National Aeronautics and Space Administration's Earth Science Research Program. All airborne data collected during the WINTER campaign by the Purdue and UMD aircraft are available on the WINTER Data Archive at EOL: http://data.eol.ucar.edu/master_list/?project=WINTER. Purdue University airborne data collected in Indianapolis as part of the INFLUX campaign are available at: http://sites.psu.edu/influx/data/. The authors declare no competing financial interest.

References

Acevedo, O. C., and D. R. Fitzjarrald (2001), The Early Evening Surface-Layer Transition: Temporal and Spatial Variability, *Journal of the Atmospheric Sciences*, *58*(17), 2650-2667, doi: 10.1175/1520-0469(2001)058<2650:teeslt>2.0.co;2.

Ackerman, B. (1987), Climatology of Chicago Area Urban-Rural Differences in Humidity, J. Clim. Appl. Meteorol., 26(3), 427-430, doi: doi:10.1175/1520-0450(1987)026<0427:COCAUR>2.0.CO;2.

Arnfield, A. J. (2003), Two decades of urban climate research: a review of turbulence, exchanges of energy and water, and the urban heat island, Int. J. Climatol., 23(1), 1-26, doi: 10.1002/joc.859.

Ao, X., C. S. B. Grimmond, Y. Chang, D. Liu, Y. Tang, P. Hu, Y. Wang, J. Zou, and J. Tan (2016), Heat, water and carbon exchanges in the tall megacity of Shanghai: challenges and results, *Int. J. Climatol.*, *36*(14), 4608-4624, doi: 10.1002/joc.4657.

Bengtsson, L., and G. Westerström (1992), Urban snowmelt and runoff in northern Sweden, Hydrol. Sci. J., 37(3), 263-275, doi: 10.1080/02626669209492586.

Berg, L., and K. J. Allwine (2006), An Analysis of Wintertime Winds in Washington, DC, edited, PNNL–15799, Pacific Northwest National Laboratory, Richland, Washington.Bergeron, O., and I. B. Strachan (2012), Wintertime radiation and energy budget along an urbanization gradient in Montreal, Canada, *Int. J. Climatol.*, *32*(1), 137-152, doi: 10.1002/joc.2246.

Bornstein, R. D., Tam, Y.-T. (1977), Anthropogenic moisture production and its effect on boundary-layer circulations over New York City, paper presented at Heisler, Gordon M.; Herrington, Lee P., eds. Proceedings of the conference on metropolitan physical environment; Gen. Tech. Rep. NE-25., Upper Darby, PA: U.S. Department of Agriculture, Forest Service, Northeastern Forest Experiment Station.

Bosilovich, M. G., S. Akella, L. Coy, R. Cullather, C. Draper, R., and R. K. Gelaro, Q. Liu, A. Molod, P. Norris, et al. (2015), MERRA-2: Initial evaluation of the climate. NASA/TM–2015–104606, 43, 139.

Brent, L. C., W. J. Thorn, M. Gupta, J. B. Leen, J. W. Stehr, H. He, H. L. Arkinson, A. Weinheimer, C. Garland, S. E. Pusede, et al. (2015), Evaluation of the use of a commercially available cavity ringdown absorption spectrometer for measuring NO2 in flight, and observations over the Mid-Atlantic States, during DISCOVER-AQ, J. Atmos. Chem., 72(3), 503-521, doi: 10.1007/s10874-013-9265-6.

Bréon, F.-M. (2006), How Do Aerosols Affect Cloudiness and Climate?, Science, 313(5787), 623-624, doi: 10.1126/science.1131668.Cambaliza, M. O. L., P. B. Shepson, D. R. Caulton, B. H. Stirm, D. Samarov, K. R. Gurney, J. Turnbull, K. J. Davis, A. Possolo, A. Karion., et al. (2014), Assessment of uncertainties of an aircraft-based mass balance approach for quantifying urban greenhouse gas emissions, Atmos. Chem. Phys., 14(17), 9029-9050, doi: 10.5194/acp-14-9029-2014.

742 Cambaliza, M. O. L., P. B. Shepson, J. Bogner, D. R. Caulton, B. H. Stirm, C. Sweeney, S. A.
743 Montzka, K. R. Gurney, K. Spokas, O. E. Salmon, et al. (2015), Quantification and source
744 apportionment of the methane emission flux from the city of Indianapolis, Elementa, 3(1),
745 000037, doi: 10.12952/journal.elementa.000037.

746 Carlton, A. G., and B. J. Turpin (2013), Particle partitioning potential of organic compounds is
747 highest in the Eastern US and driven by anthropogenic water, Atmos. Chem. Phys., 13(20),
748 10203-10214, doi: 10.5194/acp-13-10203-2013.Center for International Earth Science
749 Information Network - CIESIN - Columbia University, International Food Policy Research
750 Institute - IFPRI, The World Bank, and Centro Internacional de Agricultura Tropical - CIAT
751 (2011), *Global Rural-Urban Mapping Project, Version 1 (GRUMPv1): Population Count Grid*,
752 NASA Socioeconomic Data and Applications Center (SEDAC), Palisades, NY.

753 Chandler, T. (1967), Absolute and relative humidities in towns, Bull. Amer. Meteor. Soc., 48(6),
754 394-399.

755 Chung, E.-S., B. Soden, B. Sohn, and L. Shi (2014), Upper-tropospheric moistening in response
756 to anthropogenic warming, Proc. Natl. Acad. Sci., 111(32), 11636-11641, doi:
757 10.1073/pnas.1409659111.

758 Christen, A. (2014), Atmospheric measurement techniques to quantify greenhouse gas emissions
759 from cities, *Urban Climate*, *10, Part 2*, 241-260, doi:
760 http://dx.doi.org/10.1016/j.uclim.2014.04.006.

761 Crawford, T. L., and R. J. Dobosy (1992), A sensitive fast-response probe to measure turbulence
762 and heat flux from any airplane, Bound.-Layer Meteo., 59(3), 257-278, doi:
763 10.1007/BF00119816.

764 Deosthali, V. (2000), Impact of rapid urban growth on heat and moisture islands in Pune City,
765 India, Atmos. Environ., 34(17), 2745-2754, doi: 10.1016/S1352-2310(99)00370-2.

766 Fattouh, B. (2014), The US Shale Revolution and the Changes in LPG Trade Dynamics: A
767 Threat to the GCC?, edited, Oxford Energy Comment.

768 Font, A., C. S. B. Grimmond, S. Kotthaus, J. A. Morguí, C. Stockdale, E. O'Connor, M.
769 Priestman, and B. Barratt (2015), Daytime CO2 urban surface fluxes from airborne
770 measurements, eddy-covariance observations and emissions inventory in Greater London,
771 *Environ. Pollut.*, *196*, 98-106, doi: http://dx.doi.org/10.1016/j.envpol.2014.10.001.

772 Garman, K., K. Hill, P. Wyss, M. Carlsen, J. Zimmerman, B. Stirm, T. Carney, R. Santini, and P.
773 Shepson (2006), An Airborne and Wind Tunnel Evaluation of a Wind Turbulence Measurement
774 System for Aircraft-Based Flux Measurements*, J. Atmos. Oceanic Technol., 23(12), 1696-
775 1708, doi: http://dx.doi.org/10.1175/JTECH1940.1.

776 Gioli, B., M. F. Carfora, V. Magliulo, M. C. Metallo, A. A. Poli, P. Toscano, and F. Miglietta
777 (2014), Aircraft mass budgeting to measure CO2 emissions of Rome, Italy, *Environ. Monit.*
778 *Assess.*, *186*(4), 2053-2066, doi: 10.1007/s10661-013-3517-4.

Global Modeling and Assimilation Office (GMAO) (2015a), MERRA-2 tavg3_3d_asm_Nv: 3d,3-Hourly,Time-Averaged,Model-Level,Assimilation,Assimilated Meteorological Fields V5.12.4, version 5.12.4, Greenbelt, MD, USA, Goddard Earth Sciences Data and Information Services Center (GES DISC), doi:10.5067/SUOQESM06LPK.

Global Modeling and Assimilation Office (GMAO) (2015b), MERRA-2 tavg1_2d_slv_Nx: 2d,1-Hourly,Time-Averaged,Single-Level,Assimilation,Single-Level Diagnostics V5.12.4, version 5.12.4, Greenbelt, MD, USA, Goddard Earth Sciences Data and Information Services Center (GES DISC), doi:10.5067/VJAFPLI1CSIV.

Gorski, G., C. Strong, S. P. Good, R. Bares, J. R. Ehleringer, and G. J. Bowen (2015), Vapor hydrogen and oxygen isotopes reflect water of combustion in the urban atmosphere, Proc. Natl. Acad. Sci., 112(11), 3247-3252, doi: 10.1073/pnas.1424728112.

Grimmond, C. S. B. (1992), The suburban energy balance: Methodological considerations and results for a mid-latitude west coast city under winter and spring conditions, Int. J. Climatol., 12(5), 481-497, doi: 10.1002/joc.3370120506.

Grimmond, C. S. B., M. Blackett, M. J. Best, J. Barlow, J.-J. Baik, S. E. Belcher, S. I. Bohnenstengel, I. Calmet, F. Chen, A. Dandou, et al. (2010), The International Urban Energy Balance Models Comparison Project: First Results from Phase 1, J. Appl. Meteorol. Climatol., 49(6), 1268-1292, doi: doi:10.1175/2010JAMC2354.1.

Guo, H., L. Xu, A. Bougiatioti, K. M. Cerully, S. L. Capps, J. R. Hite Jr, A. G. Carlton, S. H. Lee, M. H. Bergin, N. L. Ng, et al. (2015), Fine-particle water and pH in the southeastern United States, Atmos. Chem. Phys., 15(9), 5211-5228, doi: 10.5194/acp-15-5211-2015.

Hage, K. (1972), Urban growth effects on low-temperature fog in Edmonton, Bound.-Layer Meteo., 2(3), 334-347, doi: 10.1007/BF02184774.

Hage, K. (1975), Urban-rural humidity differences, J. Appl. Meteorol., 14(7), 1277-1283, doi: http://dx.doi.org/10.1175/1520-0450(1975)014<1277:URHD>2.0.CO;2.

Hall, S. J., J. Learned, B. Ruddell, K. L. Larson, J. Cavender-Bares, N. Bettez, P. M. Groffman, J. M. Grove, J. B. Heffernan, S. E. Hobbie, et al. (2016), Convergence of microclimate in residential landscapes across diverse cities in the United States, Landscape Ecol., 31(1), 101-117, doi: 10.1007/s10980-015-0297-y.

Hane, C. E. (1978), The application of a 2-D convective cloud model to waste heat release from proposed nuclear energy centers, *Atmos. Environ.*, *12*(9), 1839-1848, doi: http://dx.doi.org/10.1016/0004-6981(78)90003-3.

He, H., K. Y. Vinnikov, C. Li, N. A. Krotkov, A. R. Jongeward, Z. Li, J. W. Stehr, J. C. Hains, and R. R. Dickerson (2016), Response of SO2 and particulate air pollution to local and regional emission controls: A case study in Maryland, Earth's Future, 4(4), 94-109, doi: 10.1002/2015ef000330.

He, H., C. P. Loughner, J. W. Stehr, H. L. Arkinson, L. C. Brent, M. B. Follette-Cook, M. A. Tzortziou, K. E. Pickering, A. M. Thompson, D. K. Martins, et al. (2014), An elevated reservoir of air pollutants over the Mid-Atlantic States during the 2011 DISCOVER-AQ campaign: Airborne measurements and numerical simulations, Atmos. Environ., 85, 18-30, doi: http://dx.doi.org/10.1016/j.atmosenv.2013.11.039.

Heimburger, A. M., R. M. Harvey, P. B. Shepson, B. H. Stirm, C. Gore, J. Turnbull, M. O. Cambaliza, O. E. Salmon, A.-E. M. Kerlo, and T. N. Lavoie (2017), Assessing the optimized precision of the aircraft mass balance method for measurement of urban greenhouse gas emission rates through averaging, *Elem Sci Anth*, *5*, doi: http://doi.org/10.1525/elementa.134.Hicks, B. B., W. J. Callahan, and M. A. Hoekzema (2010), On the Heat Islands of Washington, DC, and New York City, NY, Bound.-Layer Meteo., 135(2), 291-300, doi: 10.1007/s10546-010-9468-1.

Ho, C., and C. Valeo (2005), Observations of urban snow properties in Calgary, Canada, Hydrol. Processes, 19(2), 459-473, doi: 10.1002/hyp.5544.

Hodas, N., A. P. Sullivan, K. Skog, F. N. Keutsch, J. L. Collett Jr, S. Decesari, M. C. Facchini, A. G. Carlton, A. Laaksonen, and B. J. Turpin (2014), Aerosol liquid water driven by anthropogenic nitrate: Implications for lifetimes of water-soluble organic gases and potential for secondary organic aerosol formation, Environ. Sci. Technol., 48(19), 11127-11136, doi: 10.1021/es5025096.

Holmer, B., and I. Eliasson (1999), Urban–rural vapour pressure differences and their role in the development of urban heat islands, Int. J. Climatol., 19(9), 989-1009, doi: 10.1002/(sici)1097-0088(199907)19:9<989::aid-joc410>3.0.co;2-1.

Järvi, L., C. S. B. Grimmond, M. Taka, A. Nordbo, H. Setälä, and I. B. Strachan (2014), Development of the Surface Urban Energy and Water Balance Scheme (SUEWS) for cold climate cities, Geosci. Model Dev., 7(4), 1691-1711, doi: 10.5194/gmd-7-1691-2014.

Kalanda, B., T. R. Oke, and D. Spittlehouse (1980), Suburban energy balance estimates for Vancouver, BC, using the Bowen ratio-energy balance approach, J. Appl. Meteorol., 19(7), 791-802, doi: 10.1175/1520-0450(1980)019<0791:SEBEFV>2.0.CO;2.

Kalthoff, N., U. Corsmeier, K. Schmidt, C. Kottmeier, F. Fiedler, M. Habram, and F. Slemr (2002), Emissions of the city of Augsburg determined using the mass balance method, *Atmos. Environ.*, *36, Supplement 1*, 19-31, doi: http://dx.doi.org/10.1016/S1352-2310(02)00215-7.

Karion, A., C. Sweeney, G. Pétron, G. Frost, R. Michael Hardesty, J. Kofler, B. R. Miller, T. Newberger, S. Wolter, and R. Banta (2013), Methane emissions estimate from airborne measurements over a western United States natural gas field, Geophys. Res. Lett., 40(16), 4393-4397, doi: 10.1002/grl.50811.

Karion, A., C. Sweeney, E. A. Kort, P. B. Shepson, A. Brewer, M. Cambaliza, S. A. Conley, K. Davis, A. Deng, M. Hardesty, et al. (2015), Aircraft-Based Estimate of Total Methane Emissions from the Barnett Shale Region, Environ. Sci. Technol., 49(13), 8124-8131, doi: 10.1021/acs.est.5b00217.

853 Karl, T., E. Apel, A. Hodzic, D. D. Riemer, D. R. Blake, and C. Wiedinmyer (2009), Emissions
854 of volatile organic compounds inferred from airborne flux measurements over a megacity,
855 *Atmos. Chem. Phys.*, *9*(1), 271-285, doi: 10.5194/acp-9-271-2009.

856 Kopec, R. J. (1973), Daily spatial and secular variations of atmospheric humidity in a small city,
857 J. Appl. Meteorol., 12(4), 639-648, doi: 10.1175/1520-
858 0450(1973)012<0639:DSASVO>2.0.CO;2.

859 Kourtidis, K., S. Stathopoulos, A. K. Georgoulias, G. Alexandri, and S. Rapsomanikis (2015), A
860 study of the impact of synoptic weather conditions and water vapor on aerosol–cloud
861 relationships over major urban clusters of China, Atmos. Chem. Phys., 15(19), 10955-10964,
862 doi: 10.5194/acp-15-10955-2015.

863 Kreidenweis, S. M., K. Koehler, P. J. DeMott, A. J. Prenni, C. Carrico, and B. Ervens (2005),
864 Water activity and activation diameters from hygroscopicity data - Part I: Theory and application
865 to inorganic salts, Atmos. Chem. Phys., 5(5), 1357-1370, doi: 10.5194/acp-5-1357-2005.

866 Kuttler, W., S. Weber, J. Schonnefeld, and A. Hesselschwerdt (2007), Urban/rural atmospheric
867 water vapour pressure differences and urban moisture excess in Krefeld, Germany, Int. J.
868 Climatol., 27(14), 2005-2015, doi: 10.1002/joc.1558.

869 Lauvaux, T., N. L. Miles, A. Deng, S. J. Richardson, M. O. Cambaliza, K. J. Davis, B. Gaudet,
870 K. R. Gurney, J. Huang, D. O'Keefe, et al. (2016), High-resolution atmospheric inversion of
871 urban CO2 emissions during the dormant season of the Indianapolis Flux Experiment
872 (INFLUX), J. Geophys. Res.: Atmos., 121(10), 5213-5236, doi: 10.1002/2015jd024473.

873 Lavoie, T. N., P. B. Shepson, M. O. Cambaliza, B. H. Stirm, A. Karion, C. Sweeney, T. I.
874 Yacovitch, S. C. Herndon, X. Lan, and D. Lyon (2015), Aircraft-based measurements of point
875 source methane emissions in the Barnett Shale basin, Environ. Sci. Technol., 49(13), 7904-7913,
876 doi: 10.1021/acs.est.5b00410.

877 Lemonsu, A., S. Bélair, J. Mailhot, M. Benjamin, G. Morneau, B. Harvey, F. Chagnon, M. Jean,
878 and J. Voogt (2008), Overview and First Results of the Montreal Urban Snow Experiment 2005,
879 *J. Appl. Meteorol. Climatol.*, *47*(1), 59-75, doi: 10.1175/2007jamc1639.1.

880 Leroyer, S., J. Mailhot, S. Bélair, A. Lemonsu, and I. B. Strachan (2010), Modeling the Surface
881 Energy Budget during the Thawing Period of the 2006 Montreal Urban Snow Experiment, *J.*
882 *Appl. Meteorol. Climatol.*, *49*(1), 68-84, doi: 10.1175/2009jamc2153.1.

883 Liu, W., H. You, and J. Dou (2009), Urban-rural humidity and temperature differences in the
884 Beijing area, Theor. Appl. Climatol., 96(3), 201-207, doi: 10.1007/s00704-008-0024-6.

885 Lothon, M., F. Lohou, D. Pino, F. Couvreux, E. R. Pardyjak, J. Reuder, J. Vilà-Guerau de
886 Arellano, P. Durand, O. Hartogensis, D. Legain, et al. (2014), The BLLAST field experiment:
887 Boundary-Layer Late Afternoon and Sunset Turbulence, *Atmos. Chem. Phys.*, *14*(20), 10931-
888 10960, doi: 10.5194/acp-14-10931-2014.

889 Mays, K. L., P. B. Shepson, B. H. Stirm, A. Karion, C. Sweeney, and K. R. Gurney (2009),
890 Aircraft-based measurements of the carbon footprint of Indianapolis, Environ. Sci. Technol.,
891 43(20), 7816-7823, doi: 10.1021/es901326b.

892 McCarthy, M. P., M. J. Best, and R. A. Betts (2010), Climate change in cities due to global
893 warming and urban effects, Geophys. Res. Lett., 37, doi: 10.1029/2010gl042845.

894 McKain, K., A. Down, S. M. Raciti, J. Budney, L. R. Hutyra, C. Floerchinger, S. C. Herndon, T.
895 Nehrkorn, M. S. Zahniser, and R. B. Jackson (2015), Methane emissions from natural gas
896 infrastructure and use in the urban region of Boston, Massachusetts, Proc. Natl. Acad. Sci.,
897 112(7), 1941-1946, doi: 10.1073/pnas.1416261112.

898 Meroney, R. N. (2006), CFD prediction of cooling tower drift, Journal of Wind Engineering and
899 Industrial Aerodynamics, 94(6), 463-490, doi: http://dx.doi.org/10.1016/j.jweia.2006.01.015.

900 Mlawer, E. J., S. J. Taubman, P. D. Brown, M. J. Iacono, and S. A. Clough (1997), Radiative
901 transfer for inhomogeneous atmospheres: RRTM, a validated correlated-k model for the
902 longwave, J. Geophys. Res.: Atmos., 102(D14), 16663-16682, doi: 10.1029/97JD00237.

903 Mölders, N., and M. A. Olson (2004), Impact of Urban Effects on Precipitation in High
904 Latitudes, *Journal of Hydrometeorology*, *5*(3), 409-429, doi: 10.1175/1525-
905 7541(2004)005<0409:ioueop>2.0.co;2.

906 Moore, J., and A. D. Jacobson (2015), Seasonally varying contributions to urban CO2 in the
907 Chicago, Illinois, USA region: Insights from a high-resolution CO2 concentration and δ13C
908 record, Elementa, 3(1), 000052, doi: 10.12952/journal.elementa.000052.

909 Moriwaki, R., and M. Kanda (2004), Seasonal and diurnal fluxes of radiation, heat, water vapor,
910 and carbon dioxide over a suburban area, J. Appl. Meteorol., 43(11), 1700-1710, doi:
911 10.1175/JAM2153.1.

912 Moriwaki, R., M. Kanda, H. Senoo, A. Hagishima, and T. Kinouchi (2008), Anthropogenic
913 water vapor emissions in Tokyo, Water Resour. Res., 44(11), doi: 10.1029/2007WR006624.

914 National Weather Service (2016), Indianapolis and Washington, D.C.-Baltimore Climatological
915 Information. November 2012 to March 2015. www.weather.gov. National Oceanic and
916 Atmospheric Administration and National Weather Service. [Updated daily.]

917 Neumann, N., and P. Marsh (1998), Local advection of sensible heat in the snowmelt landscape
918 of Arctic tundra, Hydrol. Processes, 12(10-11), 1547-1560, doi: 10.1002/(SICI)1099-
919 1085(199808/09)12:10/11<1547::AID-HYP680>3.0.CO;2-Z.

920 Nguyen, T. K. V., S. L. Capps, and A. G. Carlton (2015), Decreasing Aerosol Water Is
921 Consistent with OC Trends in the Southeast US, Environ. Sci. Technol., 49(13), 7843-7850, doi:
922 10.1021/acs.est.5b00828.

923 Oke, T. (1979), Advectively-assisted evapotranspiration from irrigated urban vegetation, Bound.-
924 Layer Meteo., 17(2), 167-173, doi: 10.1007/BF00117976.

925 Oke, T., and J. McCaughey (1983), Suburban-rural energy balance comparisons for Vancouver,
926 BC: an extreme case?, Bound.-Layer Meteo., 26(4), 337-354, doi: 10.1007/BF00119532.

927 Oke, T., G. Zeuner, and E. Jauregui (1992), The surface energy balance in Mexico City, Atmos.
928 Environ., 26(4), 433-444, doi: 10.1016/0957-1272(92)90050-3.

929 Oke, T., G. Johnson, D. Steyn, and I. Watson (1991), Simulation of surface urban heat islands
930 under 'ideal'conditions at night part 2: diagnosis of causation, Bound.-Layer Meteo., 56(4), 339-
931 358, doi: 10.1007/BF00119211.

932 Offerle, B., C. S. B. Grimmond, K. Fortuniak, K. Kłysik, and T. R. Oke (2006), Temporal
933 variations in heat fluxes over a central European city centre, *Theor. Appl. Climatol.*, *84*(1), 103-
934 115, doi: 10.1007/s00704-005-0148-x.

935 O'Shea, S. J., G. Allen, Z. L. Fleming, S. J. B. Bauguitte, C. J. Percival, M. W. Gallagher, J. Lee,
936 C. Helfter, and E. Nemitz (2014), Area fluxes of carbon dioxide, methane, and carbon monoxide
937 derived from airborne measurements around Greater London: A case study during summer 2012,
938 *J. Geophys. Res.: Atmos.*, *119*(8), 4940-4952, doi: 10.1002/2013jd021269.

939 Orville, H. D., P. A. Eckhoff, J. E. Peak, J. H. Hirsch, and F. J. Kopp (1981), Numerical
940 simulation of the effects of cooling tower complexes on clouds and severe storms, *Atmos.*
941 *Environ.*, *15*(5), 823-836, doi: http://dx.doi.org/10.1016/0004-6981(81)90287-0.

942 Pétron, G., A. Karion, C. Sweeney, B. R. Miller, S. A. Montzka, G. J. Frost, M. Trainer, P. Tans,
943 A. Andrews, and J. Kofler (2014), A new look at methane and nonmethane hydrocarbon
944 emissions from oil and natural gas operations in the Colorado Denver-Julesburg Basin, J.
945 Geophys. Res.: Atmos., 119(11), 6836-6852, doi: 10.1002/2013JD021272.

946 Ramamurthy, P., E. Bou-Zeid, J. A. Smith, Z. Wang, M. L. Baeck, N. Z. Saliendra, J. L. Hom,
947 and C. Welty (2014), Influence of Subfacet Heterogeneity and Material Properties on the Urban
948 Surface Energy Budget, *J. Appl. Meteorol. Climatol.*, *53*(9), 2114-2129, doi: 10.1175/jamc-d-13-
949 0286.1.

950 Richards, K. (2005), Urban and rural dewfall, surface moisture, and associated canopy-level air
951 temperature and humidity measurements for Vancouver, Canada, Bound.-Layer Meteo., 114(1),
952 143-163, doi: 10.1007/s10546-004-8947-7.

953 Rind, D., E. W. Chiou, W. Chu, J. Larsen, S. Oltmans, J. Lerner, M. P. McCormkk, and L.
954 McMaster (1991), Positive water vapour feedback in climate models confirmed by satellite data,
955 Nature, 349(6309), 500-503, doi: 10.1038/349500a0.

956 Rindelaub, J. D., K. M. McAvey, and P. B. Shepson (2015), The photochemical production of
957 organic nitrates from α-pinene and loss via acid-dependent particle phase hydrolysis, Atmos.
958 Environ., 100, 193-201, doi: 10.1016/j.atmosenv.2014.11.010.

959 Rosenfeld, D., U. Lohmann, G. B. Raga, C. D. O'Dowd, M. Kulmala, S. Fuzzi, A. Reissell, and
960 M. O. Andreae (2008), Flood or Drought: How Do Aerosols Affect Precipitation?, Science,
961 321(5894), 1309-1313, doi: 10.1126/science.1160606.

962 Ruiz, J., A. S. Kaiser, M. Ballesta, A. Gil, and M. Lucas (2013), Experimental measurement of
963 cooling tower emissions using image processing of sensitive papers, Atmos. Environ., 69, 170-
964 181, doi: http://dx.doi.org/10.1016/j.atmosenv.2012.12.014.

965 Sailor, D. J. (2011), A review of methods for estimating anthropogenic heat and moisture
966 emissions in the urban environment, Int. J. Climatol., 31(2), 189-199, doi: 10.1002/joc.2106.

967 Sisterson, D. L., and R. A. Dirks (1978), Structure of the daytime urban moisture field, Atmos.
968 Environ., 12(10), 1943-1949, doi: 10.1016/0004-6981(78)90129-4.

969 Solomon, S., K. H. Rosenlof, R. W. Portmann, J. S. Daniel, S. M. Davis, T. J. Sanford, and G.-K.
970 Plattner (2010), Contributions of stratospheric water vapor to decadal changes in the rate of
971 global warming, Science, 327(5970), 1219-1223, doi: 10.1126/science.1182488.

972 Stockham, J. (1971), Cooling Tower Study, Contract CPA 22-69-122 Rep. IITRI Project C6187,
973 IIT Research Institute, Chicago, IL.

974 Stull, R. B. (1988), An introduction to boundary layer meteorology, Springer Science & Business
975 Media.

976 Trainer, M., B. Ridley, M. Buhr, G. Kok, J. Walega, G. Hübler, D. Parrish, and F. Fehsenfeld
977 (1995), Regional ozone and urban plumes in the southeastern United States: Birmingham, a case
978 study, J. Geophys. Res.: Atmos., 100(D9), 18823-18834, doi: 10.1029/95JD01641.

979 Trousdell, J. F., S. A. Conley, A. Post, and I. C. Faloona (2016), Observing entrainment mixing,
980 photochemical ozone production, and regional methane emissions by aircraft using a simple
981 mixed-layer framework, *Atmos. Chem. Phys.*, *16*(24), 15433-15450, doi: 10.5194/acp-16-15433-
982 2016.

983 Trusilova, K., M. Jung, G. Churkina, U. Karstens, M. Heimann, and M. Claussen (2008),
984 Urbanization Impacts on the Climate in Europe: Numerical Experiments by the PSU–NCAR
985 Mesoscale Model (MM5), J. Appl. Meteorol. Climatol., 47(5), 1442-1455, doi:
986 10.1175/2007jamc1624.1.

987 Twohy, C. H., J. A. Coakley, and W. R. Tahnk (2009), Effect of changes in relative humidity on
988 aerosol scattering near clouds, J. Geophys. Res.: Atmos., 114(D5), doi: 10.1029/2008JD010991.

989 United Nations (UN) Human Settlements Programme (2011), Cities and Climate Change: Global
990 Report on Human Settlement 2011,
991 http://mirror.unhabitat.org/downloads/docs/E_Hot_Cities.pdf; UN, Nairobi, Kenya.

992 U.S. Census Bureau, Population Division (2010), CBSA Report Chapter 3 Data, U.S. Census
993 Bureau, Washington, D.C.

994 U.S. Census Bureau, Population Division (2016), Annual Estimates of the Resident Population
995 April 1, 2010 to July 1, 2015,
996 http://factfinder.census.gov/faces/tableservices/jsf/pages/productview.xhtml?src=bkmk, U.S.
997 Census Bureau, Washington, D.C.

998 U.S. Energy Information Administration (EIA) (2015), Monthly Energy Review; February to
999 March 2015, DOE/EIA-0484, http://www.eia.gov/electricity/data/browser/, U.S. EIA, Off. Of
1000 Energy Analysis, U.S. Dep. of Energy, Washington, D. C.

1001 U.S. Energy Information Administration (EIA) (2016a), State Profile and Energy Estimates,
1002 http://www.eia.gov/state/, U.S. EIA, Off. Of Energy Analysis, U.S. Dep. of Energy, Washington,
1003 D. C.

1004 U.S. Energy Information Administration (EIA) (2016b), Form EIA-860, 2015ER*,
1005 https://www.eia.gov/electricity/data/eia860/, U.S. EIA, Off. Of Energy Analysis, U.S. Dep. of
1006 Energy, Washington, D. C.

1007 U.S. Environmental Protection Agency (EPA) (1998), Compilation of Air Pollutant Emission
1008 Factors, AP 42, Fifth Edition, Volume I, Chapter 1.4 Natural Gas Combustion,
1009 http://www3.epa.gov/ttnchie1/ap42/ch01/final/c01s04.pdf , EPA, Washington, D.C.

1010 U.S. Environmental Protection Agency (EPA) (2015), Inventory of U.S. Greenhouse Gas
1011 Emissions and Sinks: 1990-2013, https://www.epa.gov/ghgemissions/sources-greenhouse-gas-
1012 emissions, EPA, Washington, D.C.

1013 Vaughan, A. R., J. D. Lee, P. K. Misztal, S. Metzger, M. D. Shaw, A. C. Lewis, R. M. Purvis, D.
1014 C. Carslaw, A. H. Goldstein, C. N. Hewitt, et al. (2016), Spatially resolved flux measurements of
1015 NOx from London suggest significantly higher emissions than predicted by inventories, *Faraday*
1016 *Discuss.*, *189*(0), 455-472, doi: 10.1039/c5fd00170f.

1017 Ward, H. C., J. G. Evans, and C. S. B. Grimmond (2013), Multi-season eddy covariance
1018 observations of energy, water and carbon fluxes over a suburban area in Swindon, UK, *Atmos.*
1019 *Chem. Phys.*, *13*(9), 4645-4666, doi: 10.5194/acp-13-4645-2013.

1020 Weston, K. C. (2000), Energy conversion–the ebook, University of Tulsa.

1021 Willett, K. M., N. P. Gillett, P. D. Jones, and P. W. Thorne (2007), Attribution of observed
1022 surface humidity changes to human influence, Nature, 449(7163), 710-712, doi:
1023 http://www.nature.com/nature/journal/v449/n7163/suppinfo/nature06207_S1.html.

1024 World Health Organization (WHO) (2016), Global Health Observatory (GHO) data,
1025 http://www.who.int/gho/urban_health/en/, WHO, Geneva, Switzerland.

Tables

Flight date	Precipitation amount in week prior to flight	Max enhancement in urban H_2O_v mole fraction relative to background [mmol mol^{-1}]	ER_{Urban} (±1σ) [kg H_2O_v s^{-1}]	ER_{Urban}:ER_{Total}
8 Nov 2012*	4 mm	0.72	$2.1 (\pm 1.2) \times 10^4$	2.6%
25 Nov 2014*	54 mm	0.65	$3.5 (\pm 1.4) \times 10^4$	3.0%
13 Feb 2015†	3 mm	0.31	$1.6 (\pm 0.66) \times 10^4$	1.7%
20 Feb 2015†	14 mm	0.24	$6.5 (\pm 2.8) \times 10^4$	8.4%
27 Feb 2015†	25 mm	1.49	$1.7 (\pm 0.81) \times 10^5$	5.9%
9 Mar 2015†	23 mm	1.09	$3.4 (\pm 1.6) \times 10^4$	1.5%
12 Mar 2015†	23 mm	0.78	$3.6 (\pm 1.6) \times 10^4$	3.1%

Table 1. Urban H_2O_v emission rate (ER_{Urban}) estimates, maximum observed urban H_2O_v enhancement, and percent contribution of urban-derived H_2O_v to the total transport of atmospheric boundary layer H_2O_v (ER_{Total}) out of the study sites for days when an elevated urban H_2O_v signal was observed. Also included is the precipitation amount reported in the seven days prior to the flight days by the Indianapolis International Airport for Indianapolis flights, and the average values reported by Washington National and Baltimore-Washington International Airports for D.C.-Balt flights. Precipitation amounts for snow events are reported in snow water equivalent.

* Indianapolis

† D.C.-Balt

Flight date (low/high surface temp)	$ER_{Combust}$ [kg H_2O_v s^{-1}]	$ER_{Combust}$:ER_{Urban} [%]	$ER_{Combust}$:ER_{Total} [%]	ER_{MaxCT} [kg H_2O_v s^{-1}]	ER_{MaxCT}:ER_{Urban} [%]	ER_{MaxCT}:ER_{Total} [%]
8 Nov 2012* (-2.8°C/8.9°C)	3.7×10^2	1.8%	0.046%	6.7×10^2	3.2%	0.084%
25 Nov 2014* (-3.3°C/2.2°C)	3.2×10^2	0.9%	0.027%	6.7×10^2	1.9%	0.056%
13 Feb 2015† (-10.3°C/-1.9°C)	1.5×10^3	9.6%	0.17%	7.4×10^3	43%	0.75%
20 Feb 2015† (-16.1°C/-6.7°C)	2.5×10^3	3.9%	0.32%	7.4×10^3	11%	0.87%
27 Feb 2015† (-6.4°C/2.5°C)	1.7×10^3	1.0%	0.057%	7.4×10^3	4.4%	0.25%
9 Mar 2015† (0.8°C/16.4°C)	6.7×10^2	2.0%	0.028%	7.4×10^3	21%	0.31%
12 Mar 2015† (3.3°C/14.4°C)	3.8×10^2	1.1%	0.029%	7.4×10^3	19%	0.56%

Table 2. Combustion-derived H_2O_v emission rate ($ER_{Combust}$) and maximum cooling tower emission rate (ER_{MaxCT}) estimates for days when an urban H_2O_v excess signal was observed, as well as the contribution of $ER_{Combust}$ and ER_{MaxCT} to ER_{Urban} (urban H_2O_v excess emission rate) and ER_{Total} (total boundary layer H_2O_v flow through study site). Also provided are the low and high surface temperatures for these days reported by the Indianapolis International Airport for Indianapolis flights or the Washington National and Baltimore-Washington International Airports for D.C.-Balt flights.

* Indianapolis

† D.C.-Balt

Figure Captions

Figure 1. The ALAR (a) flight path and (b) altitude time series on 27 February 2015. After takeoff from Manassas, VA, a vertical profile (VP1) was conducted, followed by an upwind transect (UW). Three downwind transects (DW1-3) were flown along identical waypoints perpendicular to the mean wind at 390 m, 680 m, and 930 m above sea level. Because the upwind and lowest downwind transects were conducted at the same altitude (b), only the downwind data along the lowest downwind transect is shown here for comparison purposes. A second vertical profile (VP2) was flown within the urban plume during the second downwind transect. Refueling took place approximately midway through the final downwind transect. Map source: Esri, USGS, NOAA, 2010 U.S. Census. Population density is distributed by the U.S. Census Bureau's Populated Places definitions.

Figure 2. Background H_2O_v mole fractions (cyan) are defined from air sampled along the lateral edges of the downwind transects where mole fractions are relatively constant. Observed H_2O_v mole fractions for 27 February 2015 are colored by location and altitude (in meters above sea level). Vertical dotted lines indicate the transitions between rural- and urban-influenced air.

Figure 3. Calculated urban H_2O_v excess flux (Equation 1) at each sampling point downwind of D.C.-Balt on 27 February 2015. Boundary layer height (z_i), defined as the altitude corresponding to the greatest change in $d\theta/dz$, is indicated by the horizontal dashed line. Vertical dotted lines indicate the transitions between rural- and urban-influenced air.

Figure 4. Urban plume profiles of (a) H_2O_v, (b) CO_2, (c) CH_4, (d) NO_2, and (e) aerosol observed downwind of D.C.-Balt on 27 February 2015. Transects are colored by location and altitude (in meters above sea level (msl)). (f) Comparison of aerosol number concentration along the upwind (390 msl in red) and lowest downwind transect (390 msl in black). (g) Comparison of the average normalized aerosol size distribution along the upwind transect and sections of the lowest downwind transect (sections identified in (f)).

Figure 5. Atmospheric correlation of the combustion product enhancements: H_2O_v, CO_2, and NO_2 on 27 February 2015. The data shown are background-subtracted enhancements of the atmospheric species measured within the boundary layer downwind of D.C.-Balt. The Pearson correlation coefficient (r) for the linear relationship of CO_2 and H_2O_v is $r = 0.83$.

Figure 6. Urban plumes of (a) H_2O_v, (b) CO_2, and (c) CH_4 observed downwind of Indianapolis on 8 November 2012. Urban plumes of (d) H_2O_v, (e) CO_2, and (f) CH_4 observed downwind of Indianapolis on 25 November 2014. Transects are colored by altitude (meters above ground level (m agl)). Indianapolis city boundaries are indicated by the vertical dashed lines.

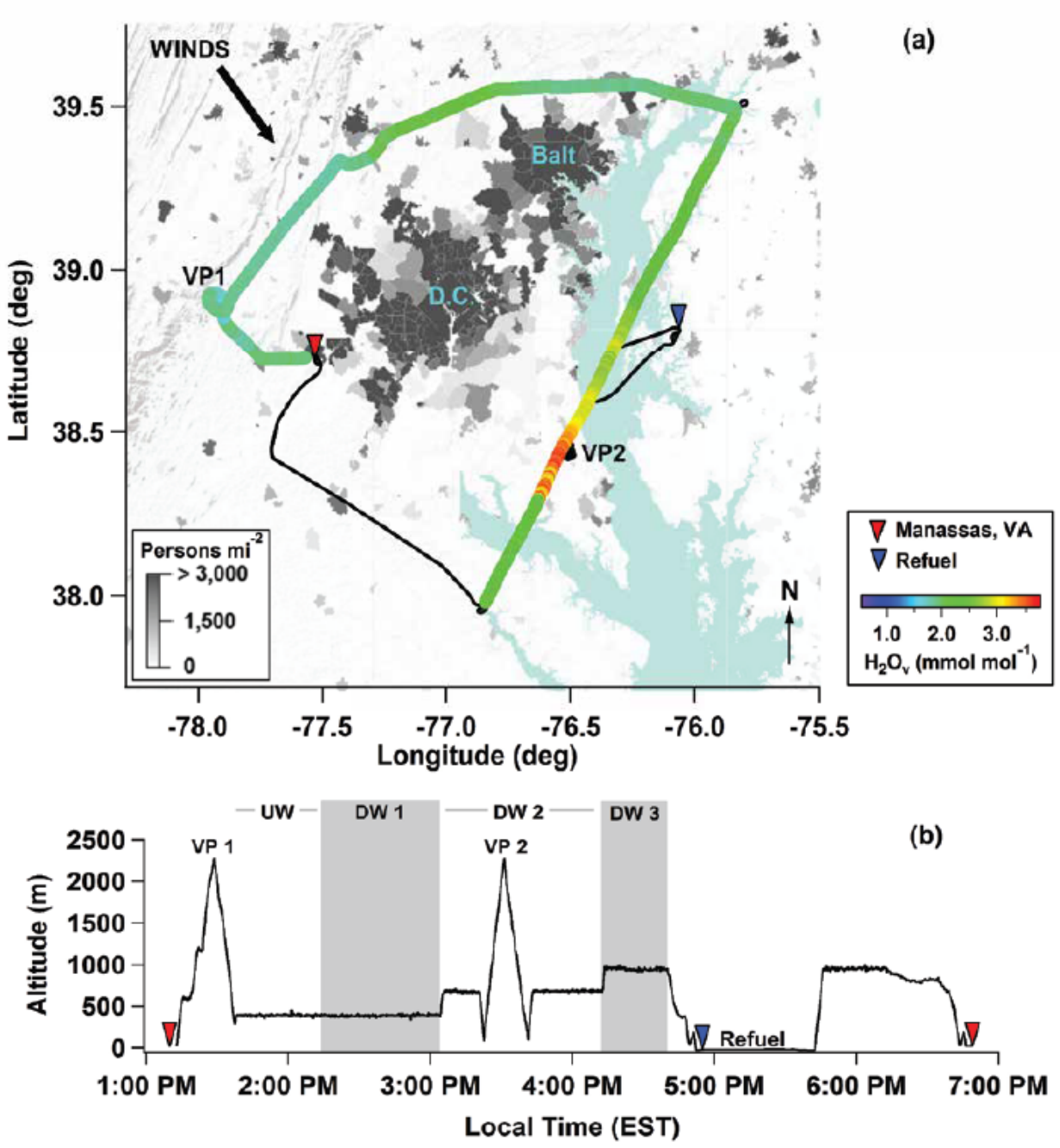

Figure 4. The ALAR (a) flight path and (b) altitude time series on 27 February 2015. After takeoff from Manassas, VA, a vertical profile (VP1) was conducted, followed by an upwind transect (UW). Three downwind transects (DW1-3) were flown along identical waypoints perpendicular to the mean wind at 390 m, 680 m, and 930 m above sea level. Because the upwind and lowest downwind transects were conducted at the same altitude (b), only the downwind data along the lowest downwind transect is shown here for comparison purposes. A second vertical profile (VP2) was flown within the urban plume during the second downwind transect. Refueling took place approximately midway through the final downwind transect. Map source: Esri, USGS, NOAA, 2010 U.S. Census. Population density is distributed by the U.S. Census Bureau's Populated Places definitions.

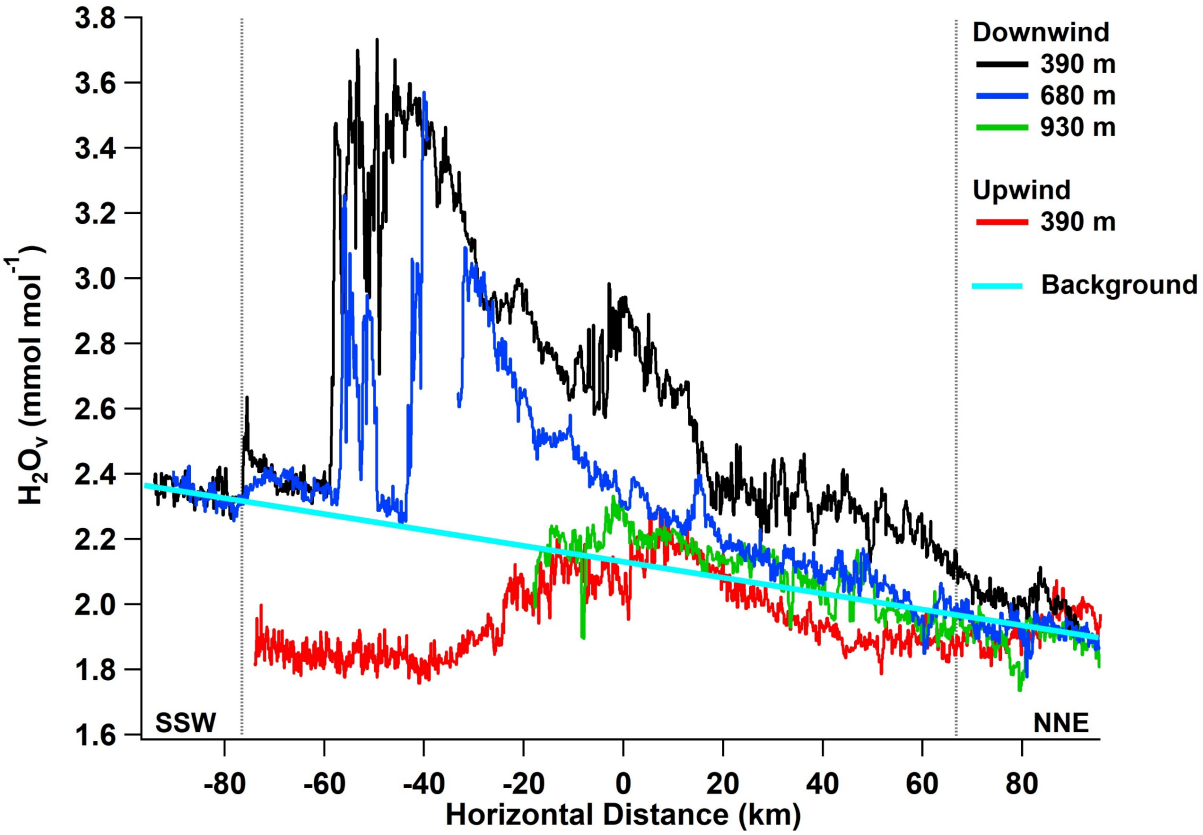

1095

1096 **Figure 5.** Background H_2O_v mole fractions (cyan) are defined from air sampled along the lateral
1097 edges of the downwind transects where mole fractions are relatively constant. Observed H_2O_v
1098 mole fractions for 27 February 2015 are colored by location and altitude (in meters above sea
1099 level). Vertical dotted lines indicate the transitions between rural- and urban-influenced air.

1100

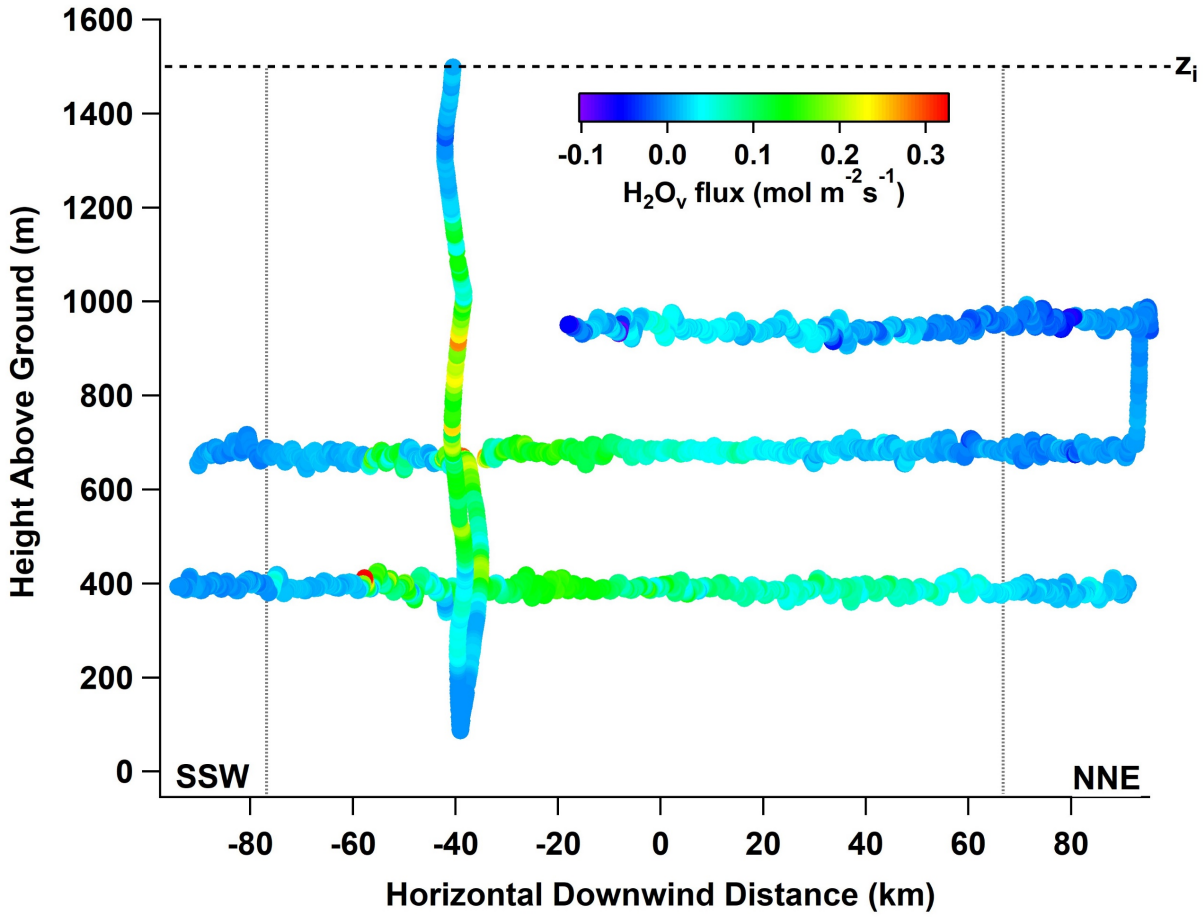

Figure 6. Calculated urban H_2O_v excess flux (Equation 1) at each sampling point downwind of D.C.-Balt on 27 February 2015. Boundary layer height (z_i), defined as the altitude corresponding to the greatest change in $d\theta/dz$, is indicated by the horizontal dashed line. Vertical dotted lines indicate the transitions between rural- and urban-influenced air.

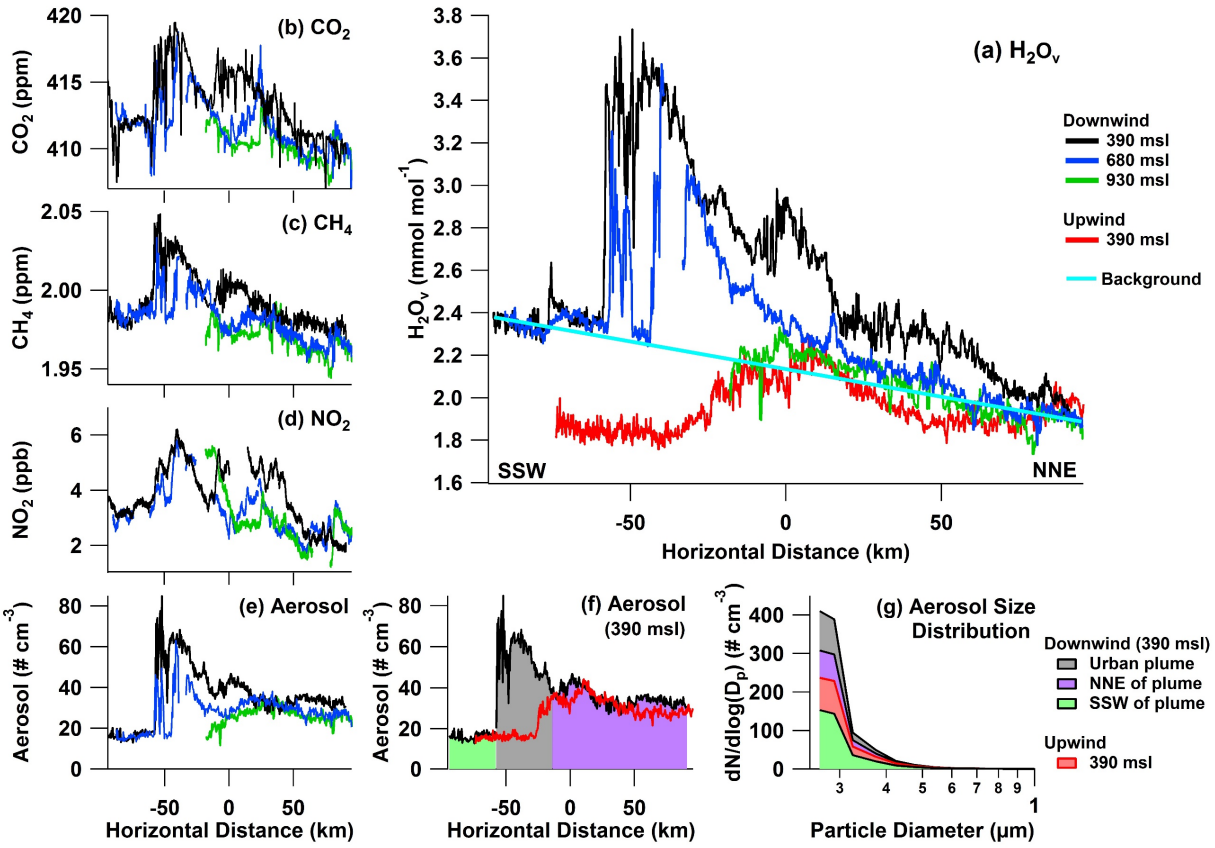

Figure 4. Urban plume profiles of (a) H_2O_v, (b) CO_2, (c) CH_4, (d) NO_2, and (e) aerosol observed downwind of D.C.-Balt on 27 February 2015. Transects are colored by location and altitude (in meters above sea level (msl)). (f) Comparison of aerosol number concentration along the upwind (390 msl in red) and lowest downwind transect (390 msl in black). (g) Comparison of the average normalized aerosol size distribution along the upwind transect and sections of the lowest downwind transect (sections identified in (f)).

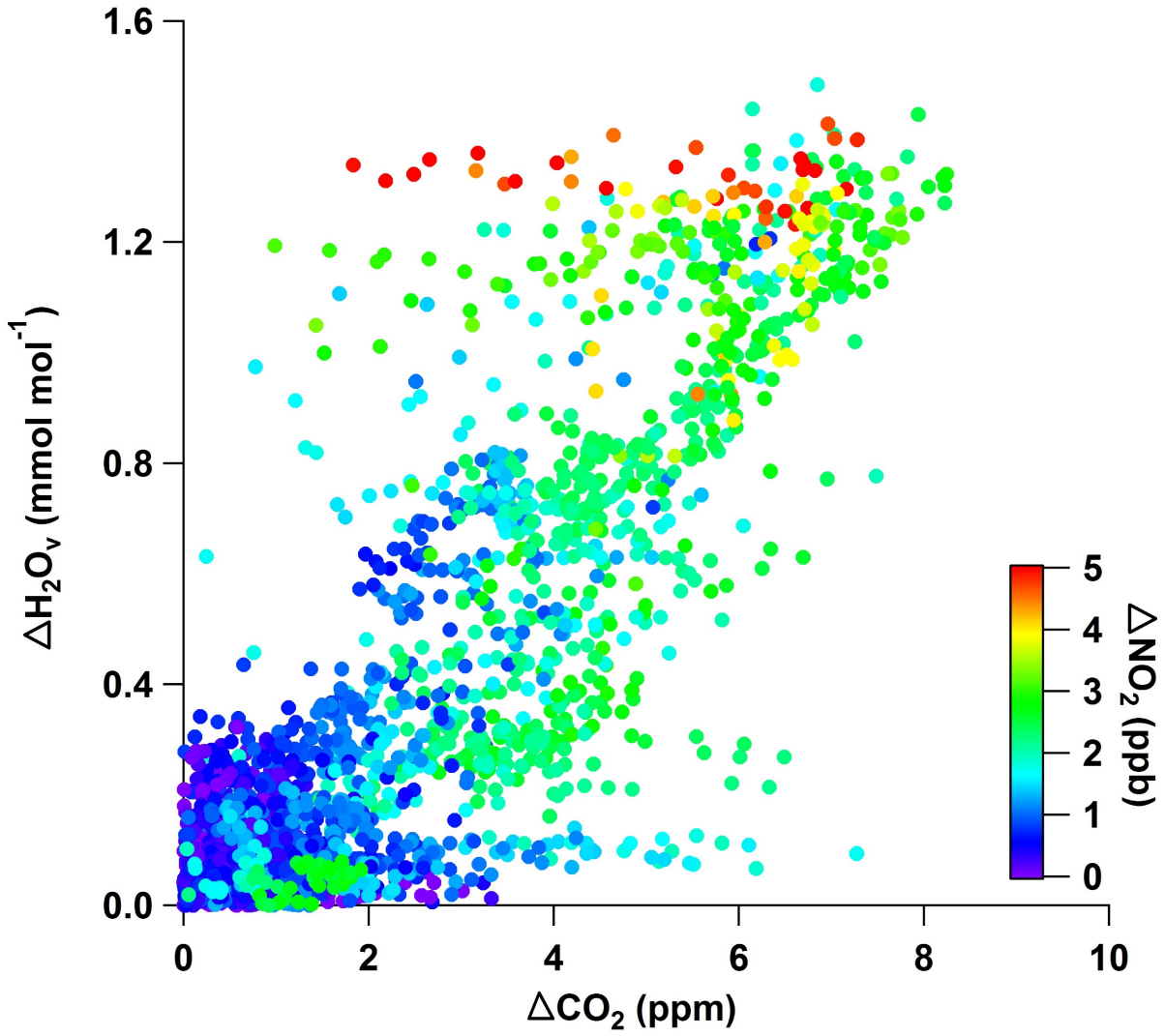

1115

1116 **Figure 5.** Atmospheric correlation of the combustion product enhancements: H_2O_v, CO_2, and
1117 NO_2 on 27 February 2015. The data shown are background-subtracted enhancements of the
1118 atmospheric species measured within the boundary layer downwind of D.C.-Balt. The Pearson
1119 correlation coefficient (r) for the linear relationship of CO_2 and H_2O_v is r = 0.83.

1120

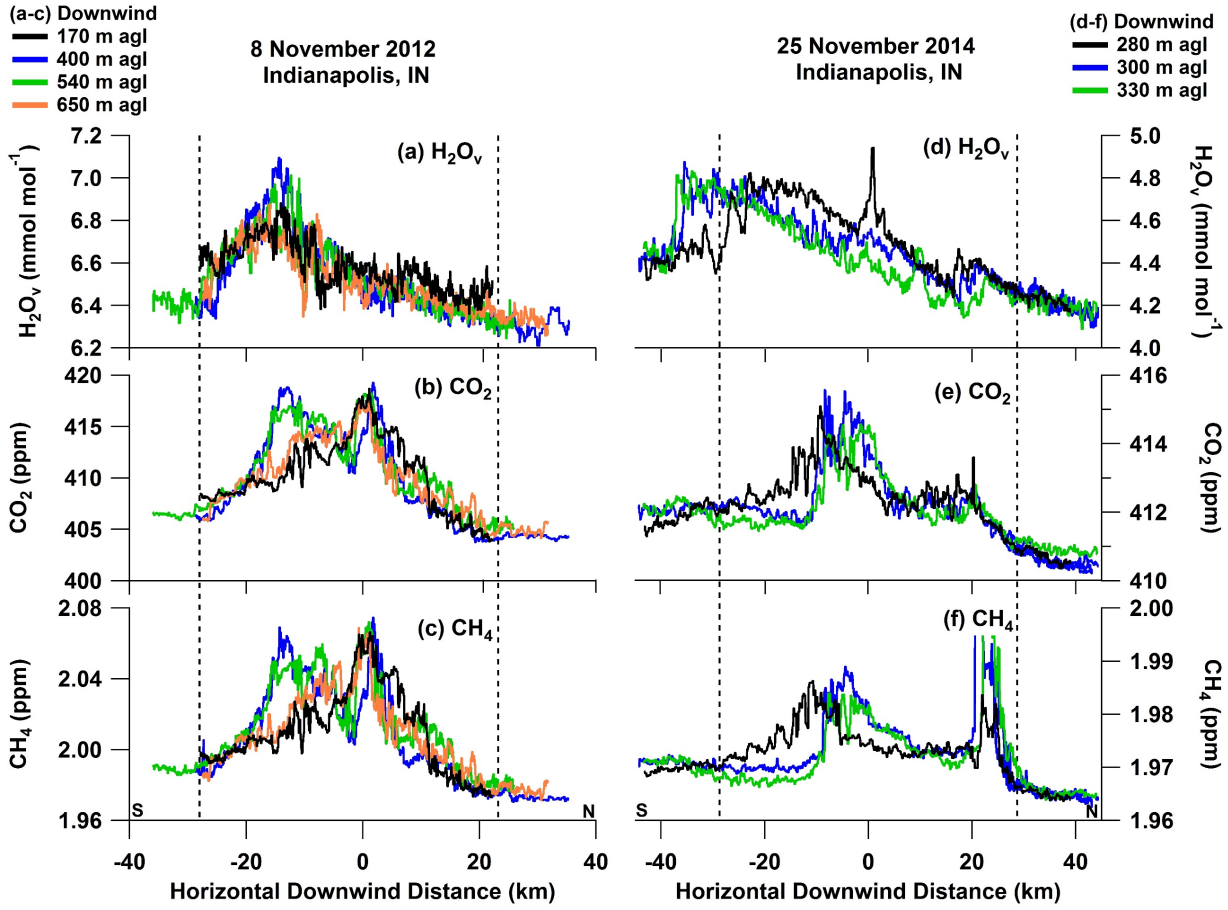

Figure 6. Urban plumes of (a) H_2O_v, (b) CO_2, and (c) CH_4 observed downwind of Indianapolis on 8 November 2012. Urban plumes of (d) H_2O_v, (e) CO_2, and (f) CH_4 observed downwind of Indianapolis on 25 November 2014. Transects are colored by altitude (meters above ground level (m agl)). Indianapolis city boundaries are indicated by the vertical dashed lines.